3. Biophysical control on particle transfer to mesopelagic depths: Results of a High Frequency Flux experiment in the Western Alboran Sea, Western Mediterranean

J. Fabres[1], A. Sanchez-Vidal[1], A. Calafat[1], M. Canals[1], S. Heussner[2] and N. Delsault[2]

[1]*GRC Geociències Marines, Dept. de Estratigrafia, Paleontologia i Geociències Marines, Universitat de Barcelona, E-08028, Barcelona, Spain*

[2]*CEntre de Formation et Recherche sur l'Environment Marin, CNRS - UMR 5110, Université de Perpignan, F-66860, Perpignan, France*

Enviat per publicació a: **Deep-Sea Research**, Octubre 2002

Abstract

As part of the MTP-II MATER project, a High Frequency Flux (HFF) experiment was carried out during spring 1998 (April-May) in the northern edge of the Western Alboran Gyre (WAG). The experiment consisted in the collection of particle flux and hydrographic data. Particle flux data came from four mooring arrays totalling seven sediment traps sampling at frequencies of 3 to 10 days. Hydrographic data consist of temporal series of current data obtained by current meters coupled to some of the sediment traps, water column properties gathered through CTD casts and water surface properties from SST and chlorophyll-a satellite imagery. Results from this experiment prove the suitability of multidisciplinary high-resolution studies to fully understand the mechanisms of biophysical coupling of particle fluxes.

Integrated analysis of particle fluxes, water column and water surface data sets reveals that in addition to high primary production along the edge of the gyre, other mechanisms mediate particle export from WAG surface waters to intermediate depths (400-500 m). These include isopycnal advection of phytoplankton rich water masses, particle aggregation and zooplankton grazing.

Disaggregation, particle size reduction and physical advection by a westward sluggish flow of intermediate and deep waters (< 4 $cm \cdot s^{-1}$) likely cause a significant decrease of particle transfer to mesopelagic depths (400-900 m). Sequestration of particulate matter across the water column is accompanied by an enhanced near bottom downslope transfer of biogenic rich material accumulated on the sea floor at shallower depths. Both processes constitute a mechanism by which carbon can be effectively removed from surface waters and driven to deep water masses or to deep-sea sediments. The later process demonstrates the potential of deep-sea sediments in the Alboran Sea to accurately record past productivity events from surface waters.

Keywords: Particulate flux, mesoscale gyres, zooplankton grazing, aggregation, nepheloid layer, Western Mediterranean Sea, Alboran Sea, (37º-35º N, 6º-3º W).

3.1. Introduction

Particle fluxes in continental margin settings and marginal seas -as the Alboran Sea in the Western Mediterranean- use to be highly variable in both total mass and composition through space and time. Three main factors account for the observed variability in the Western Alboran Sea: (i) the seasonal pattern of allochthonous particle input with variable fluvial contributions during late autumn and winter, (ii) the spatial and temporal fluctuations of the autochthonous biological production and export from the euphotic layer typically with spring to early summer and late autumn to winter pulses and, (iii) the temporal and spatial variability of dispersal and transfer processes that particles undergo before accumulating definitively on the sea bottom (Fabres et al., 2002). Furthermore, the variability of mesoscale hydrodynamic structures strongly influences particle fluxes since it controls the evolution of biological particle production, and the transfer of autochthonous and allochthonous particles.

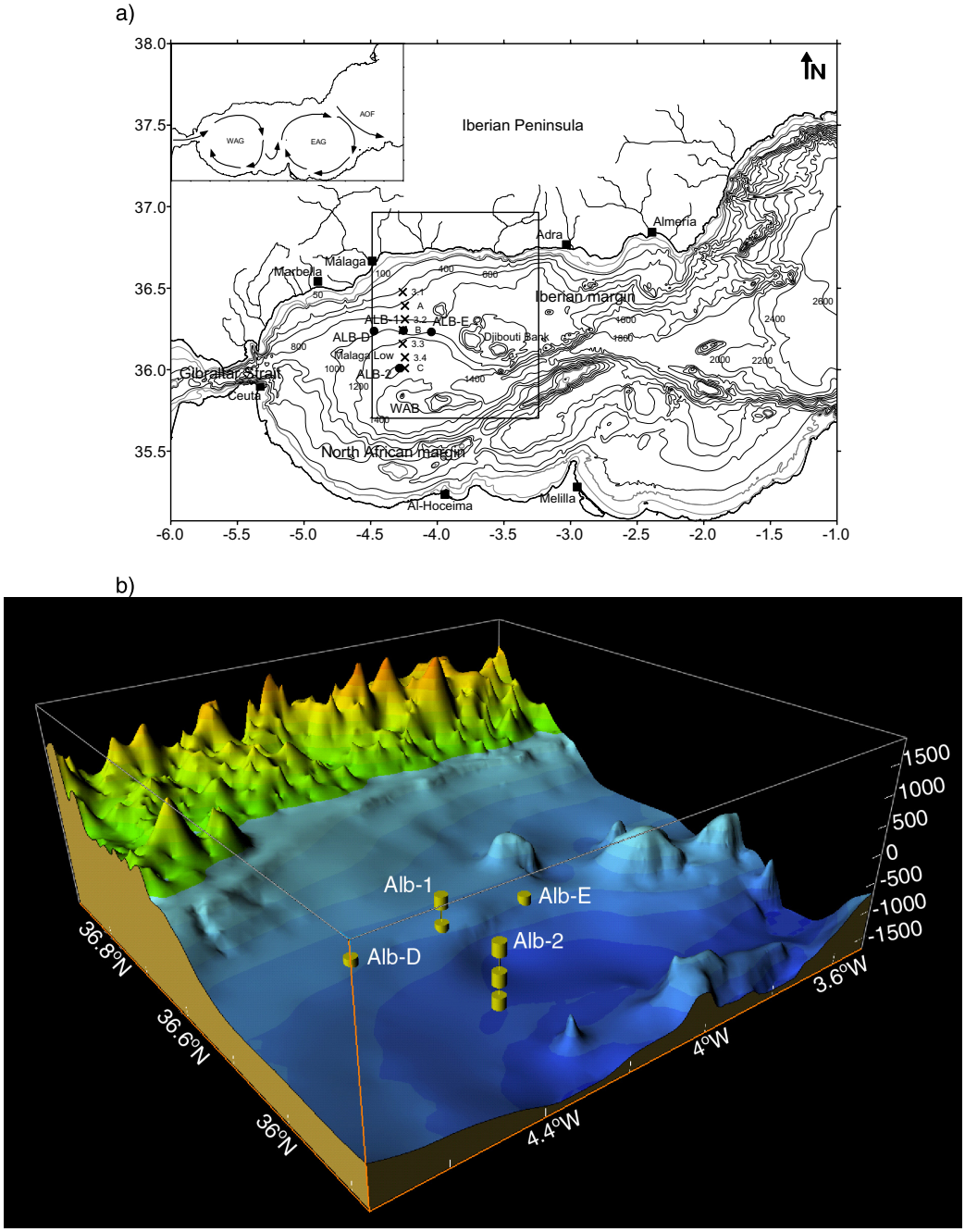

Figure 3.1. Geographical situation of the study area. a) Bathymetric map of the Alboran Sea. Isobaths are spaced 200 meters excepting the 50 and 100 meters isobaths. Black dots correspond to the four sediment trap-current meter stations and X to the CTD casts carried out the 28th of April, the 6 th of May and the 10-11th of May (WAB, Western Alboran Basin). The inset on the upper left corner outlines the surface circulation in the Alboran Sea (WAG, Western Alboran Gyre; EAG, Eastern Alboran Gyre; AOF, Almeria-Oran Front). b) Three-dimensional view from the ESE of the seafloor (blue tones) and coastal (green to orange) relieves of the study area (see box in Fig. 3.1a) showing the location of the four mooring lines with various sediment trap-current meter configurations. Vertical exaggeration is around 20. Topographic and bathymetric data from the Earth Resources Information Systems Data Center (1996) and the British Oceanographic Data Centre (1994), respectively.

The Alboran Sea is the transitional basin connecting the Atlantic Ocean and the Mediterranean Sea. Its circulation is mainly conditioned by the water exchange through the Strait of Gibraltar. This exchange involves surface (150-200 m) eastward inflow of Surface Atlantic Water (SAW, S ~36 psu at the Strait of Gibraltar), which becomes Modified Atlantic Water (MAW, S ~ 36.5-36.7 psu) through mixing and evaporation, and a westward deep outflow of a mixture of Levantine Intermediate Water (LIW, T ~13.3 ºC and S ~38.5 psu; Sparnocchia et al., 1995) and Western Mediterranean Deep Water (WMDW, T ~12.9 ºC and S ~38.4 psu; La Violette, 1995). A rather simplistic sketch (small inset in Fig. 3.1a) of the surface circulation shows two anticyclonic gyres where MAW accumulates prior to flow eastward along the Algerian margin. These anticyclonic gyres, known as the Western Alboran Gyre (WAG) and the Eastern Alboran Gyre (EAG), are on average centred on the western and eastern sectors of the Alboran Sea which are separated at about 3ºW by a set of prominent sea-floor highs with the Alboran Islet on top of one of them (Fig. 1a). Nevertheless, the surface circulation pattern is far from being stable and experiences a high temporal and spatial variability. Using satellite imagery, Heburn and La Violette (1990) were able to demonstrate the occasional disappearance of one of the gyres and large variations in their surface expression. Works devoted to the study of the spatial variability of the WAG have shown that its fluctuation periodicity is in the range of days to weeks (La Violette, 1984 and 1986; Perkins et al, 1990; Viudez et al., 1998; Garcia Lafuente et al., 1998). In the last few years, much attention has been given to the study of the vertical water mass movements in the WAB related to different mechanisms as wind, eddy-induced and/or Atlantic Jet drift upwelling (Viudez et al., 1996; Sarhan et al., 2000; Garcia-Gorriz and Carr, 2001; Gomis et al., 2001).

Biological production in surface waters is tightly linked to the evolution the mesoscale hydrodynamical structures and water column stratification (i.e. Minas et al., 1991; Garcia Lafuente et al., 1998; Rodriguez et al., 1998; Gomez et al., 2000; Moran and Estrada, 2001; Ruiz et al., 2001). Enhanced production has often been related to vertical water mass movements like those registered north-west of the WAB because of coastal upwelling, and at the periphery of the WAG because of eddy activity (Garcia-Gorriz and Carr, 1999 and 2001; Baldacci et al., 2001).

Once particles are produced, their dispersal and downward transfer and, therefore, the efficiency of the biological pump, are controlled by the evolution of the sea surface hydrodynamic conditions (i.e. Peinert and Miquel, 1994; Garcia-Gorriz and Carr, 2001; Fielding et al., 2001; Fabres et al., 2002) and the mediation of biological processes such as zooplankton grazing (Fortier et al., 1994) or phytoplankton bloom flocculation (Alldredge and Gotschalk, 1989).

Once in the near bottom environment, deep hydrodynamic conditions also play an important role in redistributing particles and transporting them to their ultimate sink (Heussner et al., 1999; Fabres et al., 2002, Masque et al., in press). Deep current data by Pistek et al. (1985), Parrilla et al., (1986) and Fabres et al. (2002) show that deep water masses flow sluggishly ($<4 m \cdot s^{-1}$) westward, specially near both the Iberian and North-African margins. Fluctuations in the speed and direction of this deep flow have a 3 to 5 day periodicity.

In the frame of the MTP-II MATER project a High Frequency Flux (HFF) experiment was performed during spring 1998 (April-May) in an area of 40x52 km located south of Malaga where the

northern edge of the WAG is most often located. The experiment consisted in the set-up of seven sediment traps coupled with current meters and the simultaneous collection of hydrographic data by direct boat observations and satellite sea surface imaging (SST and chlorophyll-a concentration). Such a high resolution experiment is embedded within a year-round particle flux monitoring study from July 1997 to May 1998 (Fabres et al., 2002). The sediment traps deployed in the experiment provide temporal series of total particle fluxes and particle composition at various depths and locations and, therefore, allow for the assessment of spatial and temporal flux variability. Furthermore, the concomitant collection of in situ hydrographic data and satellite imagery during the experiment allows tracking the evolution of the hydrodynamic structures and phytoplankton distribution. The combined use of both data sets leads to the elucidation of the links between mesoscale structures, sea-surface productivity and downward particle fluxes. This, in addition, is used to uncover the actual mechanisms controlling particle fluxes and their variability in the northern half of the Western Alboran Sea.

3.2. Data set and methodology

3.2.1. Mooring configuration

Four mooring lines, ALB-D, ALB-1, ALB-E and ALB-2, were deployed at the Iberian margin south of the coastal town of Malaga (Fig. 3.1a and Table 3.1). Three of them were deployed following a west-east section along the 36º14'N parallel above the continental slope at ~980-1000 m depth. The fourth one (ALB-2) was located 26 km south of the central mooring in the parallel transect at 1340 m depth, in a base-of-slope smooth depression named Malaga Low. All the mooring lines were equipped with a Technicap PPS3 sediment trap - Aanderaa RCM-7/RCM-8 current meter pair placed 30 m above the bottom (ALB-D-F, ALB-1-F, ALB-E-F and ALB-2-F). The aim for such a strategy was to monitor particle fluxes as near as possible to the water-sediment interface. Mooring ALB-1 contained an additional trap - current meter pair at ~480 m depth (ALB-1-S) while mooring ALB-2 included one extra trap-current meter pair at 400 m (ALB-2-S) and a single trap at ~900 m depth (ALB-2-I) (see sketch on Figure 3.1b). The aim for these later traps was to monitor particle flux evolution at intermediate depths.

Moorings were deployed on March 20th and retrieved on May 25th by R/V "Garcia del Cid". Sediment traps were programmed to collect samples from April 1st to May 22nd. For 9 of the 12 cups in PPS3 traps, a sampling frequency of 3 days each was applied from 20th of April to 16th of May. The exception were the first two cups (10 and 9 days of opening, respectively) and the last cup (6 days of opening). Such a high frequency sampling was adopted in order to resolve flux variations related with several-day long WAG fluctuations. Sample recovery within sediment trap was 100%. The design of PPS3 traps, its preparation and maintenance, and the assemblage of the mooring lines are described in Heussner et al. (1990).

Mooring line	Position		Trap code
ALB-E	Latitude	36° 13,90' N	
	Longitude	04° 02,68' W	
	Water depth	1006	
	F trap depth	**976**	**ALB-E-F**
ALB-1	Latitude	36° 14,40' N	
	Longitude	04° 15,22' W	
	Water depth	1003	
	S trap depth	**481**	**ALB-1-S**
	F trap depth	**973**	**ALB-1-F**
ALB-D	Latitude	36° 14,23' N	
	Longitude	04° 28,49' W	
	Water depth	984	
	F trap depth	**954**	**ALB-D-F**
ALB-2	Latitude	36° 00,54' N	
	Longitude	04° 17,08' W	
	Water depth	1340	
	S trap depth	**397**	**ALB-2-S**
	I trap depth	**897**	**ALB-2-I**
	F trap depth	**1307**	**ALB-2-F**

Table 3.1. Location of sediment trap-current meter pairs and traps at shallow (S), intermediate (I) and near bottom (F) depths during the April-May 1998 HFF experiment in the Western Alboran Basin.

3.2.2. Treatment of sediment trap samples

Trap receiving cups were filled with a 5% (v/v) formaldehyde solution in 0.45 μm-filtered seawater before deployment. The solution was buffered by saturation with analytical grade sodium tetraborate. The poisoning solution was used to limit degradation of settled particles, and to prevent physical disruption of swimmers. Upon recovery, trap samples were stored in the dark at 4°C before further processing in the laboratory. The analytical procedure for the determination of total mass flux, organic carbon and nitrogen, calcium carbonate, opal and lithogenic percentages is described in detail in Fabres et al. (2002). Big fishes (needlefishes) were found in the second cup of ALB-2-S and ALB-2-I. Both the low pH (< 6.5) and the unavoidable contamination by fish fragments may have caused shifts on the composition of the particulate material within the cup, a possibility that will be duly considered in the discussion section.

3.2.3. Satellite imagery

Sea Surface Temperature (SST) images used to monitor sea surface hydrology during the HFF experiment. Images were obtained from the Intelligent Satellite Data Information System (ISIS) of the Deutschen Zentrum für Luft- und Raumfahrt (DLR). These images derive from the combination of various spectral bands of the Advanced Very High-Resolution Radiometer (AVHRR) built in the NOAA satellites. Details about the algorithms used for the calculation of SST are given in McClain et al. (1985). The series of images spans from 19/03 until 25/05, and allows to draw the evolution of surface circulation

during the study period despite extensive cloud coverage during the periods 20/03–08/04 and 08/05-25/05 which caused some imagery gaps longer than 2 days. A selection of the more significant stages of this evolution is shown in Figure 3.2 (left column).

SeaWiFS (Sea-viewing Wide Field-of-view Sensor) images of chlorophyll-a concentration (mg chl-a·m^{-3}) were obtained from the Marine Environment Unit of the Space Applications Institute (Joint Research Centre, European Commission) (Melin, 2000). The series of daily images covers the Western Alboran Sea from 21/03 until 24/05, yielding a total of 18 usable images. A selection of these images as closer as possible in time to the SST images is presented in Figure 3.2 (right column). The overall image frequency of the complete series is around two days but there are several gaps of up to nine days because of orbit constrains and cloud coverage. Each individual scene is mapped onto geographical grids of 2 km resolution (Melin et al., 2000).

3.2.4. Hydrographic data

Concurrent hydrographic data were recorded during MATER-1 cruise onboard R/V Hesperides between April 28th and May 14th. Hydrographic profiles were obtained using CTD Neils Brown Mark III and Mark V profilers coupled with a Sea Tech 25 cm path length, 660 μm wavelength transmissometer and a Seatech flash lamp fluorometer. Both light transmission and fluorometry data presented here correspond to raw output voltage, which is merely a qualitative expression of the amount of particles and chlorophyll, respectively, in the water column. Three CTD transects with individual stations spaced 9 km were repeated at different times (28/04, 06/05 and 10-11/05) during the HFF experiment along the N-S transect defined by ALB-1 and ALB-2 mooring lines (Fig. 3.1a) in order to assess short-term hydrographic variability in the study area (Fig. 3.3). CTD casts of the last transect only covered from surface down to 600 m depth because of cruise time constraints.

3.2.5. Current meter data

Aanderaa RCM-7/RCM-8 current meters were deployed attached to surface (S) and bottom (F) traps to record, at an hourly frequency, current speed and direction. Table 3.2 shows the total recording period and number of days for each current meter jointly with statistic variables obtained from the records. ALB-1-S and ALB-2-F current meters recorded current direction but failed in recording current speed thus preventing calculation of residual current directions. The hourly data have been low-pass filtered with a cut-off period of 2 days to remove tidal oscillations and highlight the sub-inertial oscillations of lower frequency (Plaza, 2001) (Fig. 3.4).

Current Meter (depth)	Recording period	Days	Average speed ($cm \cdot s^{-1}$) ± stand. dev.	Maximum speed ($cm \cdot s^{-1}$)	% values > 12 $cm \cdot s^{-1}$	Residual direction (degrees from N)	Residual speed ($cm \cdot s^{-1}$)
ALB-E-F (976 m)	20/03-25/05	66	5.29 ± 3.29	19.11	3.5 %	273.19	2.74
ALB-1-F (973 m)	21/03-25/05	65	5.91 ± 4.06	22.31	9.6 %	271.47	3.31
ALB-D-F (954 m)	20/03-25/05	66	4.71 ± 2.88	15.05	1.8 %	252.49	2.82
ALB-2-S (397 m)	21/03-25/05	65	4.25 ± 2.66	12.72	0.5 %	108.29	1.85

Table 3.2. Current meter data from the April-May 1988 HFF experiment in the Western Alboran Sea.

3.3. Hydrodynamic evolution

3.3.1. Surface circulation and chlorophyll concentration from satellite imagery

The Western Alboran Sea is characterised by three thermal regimes through the year, which depend on the temperature differences between local Alboran waters and the inflowing Atlantic Jet (AJ). The inflowing waters are usually warmer than local waters from November to April ("winter" regime) and colder from July to October ("summer" regime). During the "transition" regime, from May to June, temperature differences are dimmed (Garcia-Gorriz and Carr, 1999). Hydrodynamic conditions during the studied period evolved from a winter to a summer regime under the control of three main factors: (i) the spatial evolution of the WAG, (ii) the onset and variation of the wind-induced upwelling on the northern edge of the gyre and, (iii) the eddy activity at the periphery of the gyre. SST images (Fig. 3.2, left columns) allow to differentiate incoming waters entrained by the AJ, MAW and upwelled Mediterranean waters, thus tracking the temporal evolution of surface hydrodynamic conditions during most of the studied period. SeaWiFS chlorophyll concentration images are particularly useful to track the path of the AJ and the position of the WAG during the 1998 "transition" regime, when temperature differences were lowest (Figs. 3.2d-3.2i).

Three distinct hydrographic situations were observed in the WAB during the HFF experiment The first, ranging from "winter" to the "transition" regimes, extended from 19/03 to 07/04. The WAG was restricted to the southwestern part of the WAB, displaying WNW-ESE or N-S elongated shapes with the AJ outlining the gyre while flowing eastwards. When the gyre was elongated WNW-ESE the jet headed directly south-east impinging on the Al-Hoceïma Bay off the African coastline. When the WAG was oriented N-S, the jet flowed east for a while and turned south quite abruptly impinging on the Moroccan coast west of Al-Hoceïma Bay. This period was characterised by general oligotrophic conditions with the exception of the eastern edge of the WAG, where several chlorophyll-enriched filaments developed ephemerally at the beginning of April.

The second situation, during the "transition" regime, spanned from 08/04 until 30/04 and was characterised by the fluctuating influence of cold waters upwelling to the north of the Alboran Sea. The

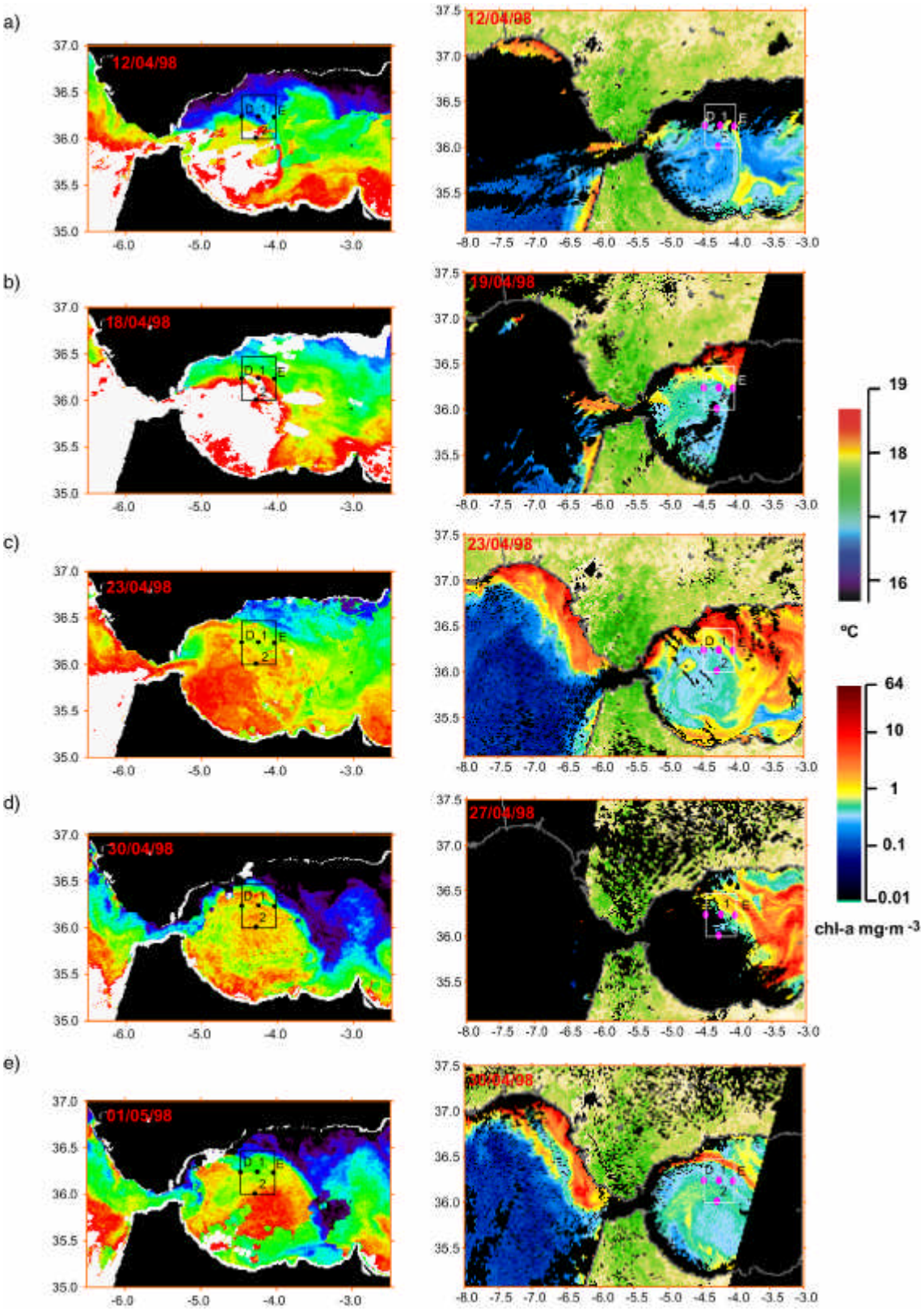

Figure 3.2. SST (ºC) and SeaWiFS (chl-a mg·m^{-3}) images of the Western Alboran Sea from mid March 1998 to mid May 1998. The succession of images is distributed in two plates. In each plate the left and the right columns correspond to SST and SeaWiFS images, respectively. The image resolution is of 1 km at nadir. For data source information see Section 3.2.3. The location of the detailed study area with the four mooring stations is also shown (box and red/black dots).

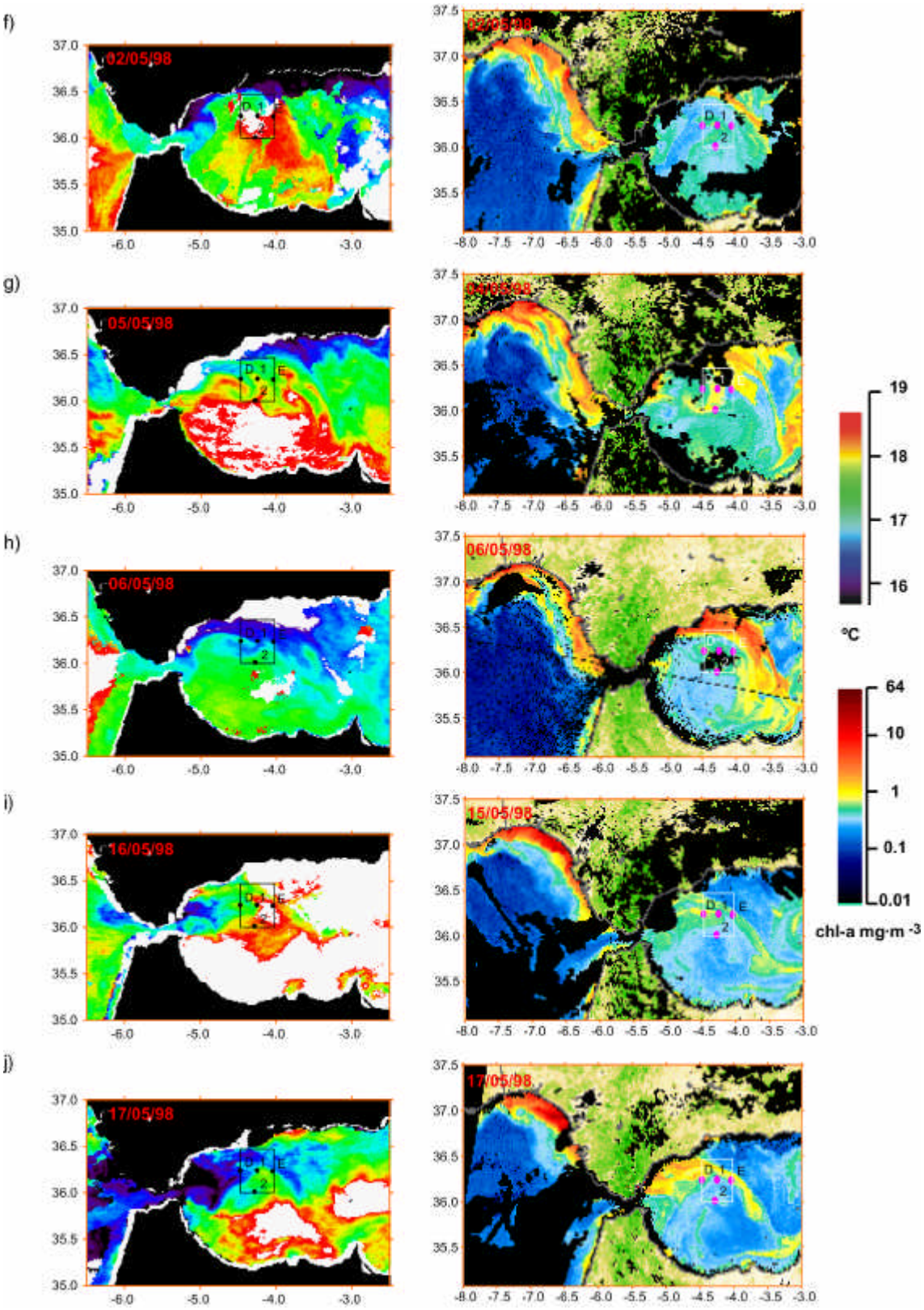

Figure 3.2. (continued)

WAG was well established, occupying most of the WAB, with its northern edge oscillating between 36º 20'N and the coast of Marbella (Figs. 3.2a-3.2d). From 12/04 to 14/04, in association to the onset of the upwelling, a noticeable increase in surface chlorophyll concentration, up to values of 10 mg·chl-a·m^{-3}, was observed on the northeastern sector of the WAB, mostly outside the WAG (Figs. 3.2b-3.2d).

The third situation, from 01/05 onwards and corresponding to the end of the "transition" regime and onset of "summer" regime, was characterised by the eastward drift of several small-scale anticyclonic eddies associated to the boundary of the WAG. On May 1st (Figs. 3.2e and 3.2f) a cold water body burst from Gibraltar Strait and spread eastwards. Such cold water body had the same characteristics than the cold-water features described by La Violette (1984). It was nourished by water upwelled just at the northeastern end of Gibraltar Strait. From 03/05 to 06/05 this cold-water feature started to develop into a small anticyclonic gyre that was advected around the outer edge of the WAG, crossing the study area between 04/05 and 06/05 (Figs. 3.2g and 3.2h). A second cold water burst was observed on May 7th but, unfortunately, cloudy conditions precluded its tracking. As seen on the SeaWiFS image of 04/05 (Fig. 3.2g), these small gyres advected phytoplankton-rich waters to the centre of the gyre. In mid May, the intensification of the entrance of waters of Atlantic origin and of the upwelling just east of Gibraltar Strait caused a south-eastwards compression of the WAG which lead almost to its collapse (Fig. 3.2j). By the end of the period, the WAG recovered its usual configuration and the small boundary eddies disappeared. Oligotrophic conditions similar to the ones recorded during the first situation were also re-established (Fig. 3.2i and 3.2j).

3.3.2. Hydrographic structure

The four near bottom and the only intermediate traps and current meters were located within the WMDW, as shown by Figure 3.3 hydrographic sections. The shallowest traps and current meters ALB-1-S and ALB-2-S were located in or slightly below the LIW core and slightly above it, respectively (Fig. 3.3).

The southward tilting of isotherms and isohalines indicates that the vertical distribution of the hydrographic variables was dominated by the gyre and upwelling mesoscale structure (Fig. 3.3). The slope and location of the 37.5 isohaline, usually chosen as the midway point between Mediterranean Water and MAW (Perkins et al., 1990), can be used to determine WAG migration. Both features clearly reflect WAG evolution from a circular shape hugging the coast of Marbella at the end of April (see Fig. 3.2) to an elongated shape displaced to the south at the beginning of May.

The 6th of May hydrographic section in Figure 3.3 mirrors another surface feature which is the fresher character of the waters forming the core of the small eddy identified on the SST images of the 5th and 6th of May (Figs. 3.2g and 3.2h). The low salinity of the eddy core indicates that these eddies engulf AJ waters.

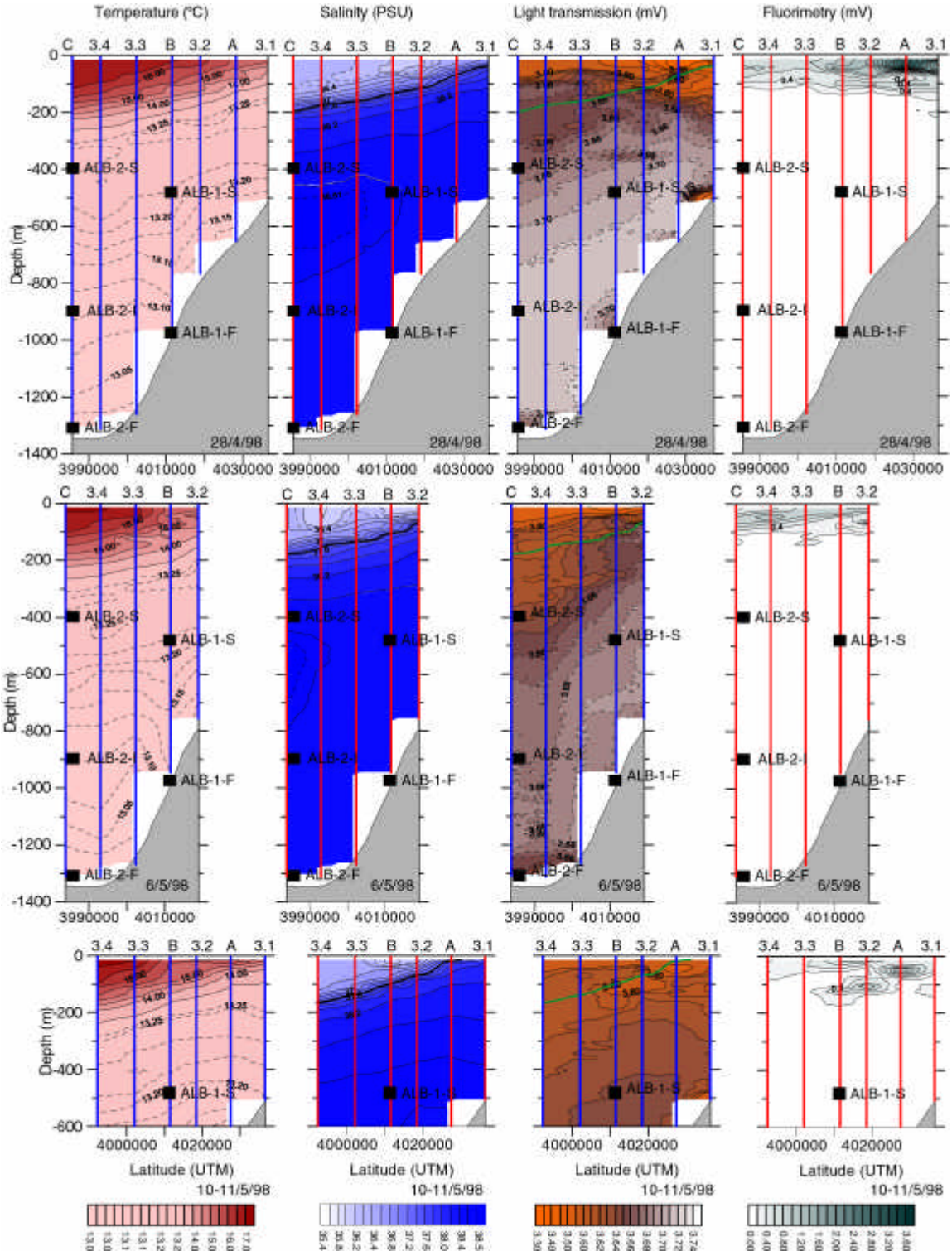

Figure 3.3. Temperature (°C), salinity (PSU), light transmission (mV) and fluorimetry (mV) vertical distributions at days 29/04, 06/05 and 10-11/05 along the same transect off Malaga across the mooring locations. Vertical bold lines and filled squares represent, respectively, CTD casts and particle trap-current meter pairs (also indicated in Figure 3.1a for reference). The 37.5 isohaline overlies the light transmission sections to facilitate comparison (see main text for details). Light transmission and fluorimetry values are given as raw output voltages.

Hydrographic sections in Figure 3.3 provide sensible information on the vertical structure of water masses filling the WAB. They show that the salinity and temperature front that develops between MAW and the underlying Mediterranean waters is not a homogeneous feature but is affected by irregularities. These irregularities are visible in all sections and especially in the 6th of May section. Temperature data clearly show bodies of colder water injected within the warmer water along the thermocline between the surface MAW and the Mediterranean waters. Allen et al. (2001) have interpreted similar temperature irregularities along the Almeria-Oran Front further east as the result of downward advection of water from the denser side of the front. Gomis et al. (2001) have suggested that this subduction mechanism would also be responsible for the southward dipping fluorescence distribution across the Malaga Front during the Omega cruise in October 1996. Such instability processes may be linked with the passage of the small eddies detected on the SST images between 01/05 and 06/05.

3.3.3. Deep circulation

Table 3.2 displays the basic statistics for current speed and direction as recorded by current meters in the moorings. At ALB-1-F and ALB-E-F the residual water flow was oriented westwards (271º-273º) with average near bottom speeds of 3.3 cm·s^{-1} and 2.7 cm·s^{-1}, respectively. Residual flow in the area where ALB-D-F was deployed headed towards the WSW (252º) with a residual speed (2.8 cm·s^{-1}) which was close to the value recorded by ALB-E-F. After plotting the directions of the residual speed vectors over a detailed bathymetric map (Fig. 3.4a), it can be seen that deep waters flow westwards following the bottom topography, and also that current intensifies over the steepest slope sections, as in ALB-1-F, probably due to fluid stretching (Cushman-Roisin, 1994). These observations are coherent with the results obtained by Pistek et al. (1985) and Parrilla et al. (1986) who described a westward sluggish flow along the northern margin of the WAB. Instantaneous speed measurements (average and maximum speed) show also a stronger current in ALB-1-F followed by ALB-E-F and ALB-D-F. The residual flow recorded by the shallowest current meter, at 400 m in ALB-2 mooring, was very sluggish and directed east-southeastwards.

Previous studies in the deep WAB have shown that collection biases due to currents potentially inducing trap tilting and loss of sampling efficiency are negligible (Fabres et al., 2002). It must be noted, however, that almost 10% of the current speed values recorded in ALB-1-F during the study period were above 12 cm·s^{-1}, the empirical threshold at which collection efficiency for cylindrical traps is reduced according to Baker et al. (1988). Nevertheless, Gardner et al. (1997) showed that fluxes collected with traps having a diameter and an aspect ratio very similar to these for PPS-3 traps used here (30.5 cm and 3 compared with 40 cm and 2.5 for the PPS-3) were only slightly biased at current speeds as high as 22 cm·s^{-1}. The possibility of collection biases due to high current speeds is further discussed in the last section of the discussion by comparing current meter data with particle flux series.

E-W and N-S components of the low pass filtered current for ALB-E-F, ALB-1-F and ALB-D-F are presented in Figure 3.4. The E-W component (Fig. 3.4b) shows higher absolute values and variability than the N-S component (Fig 3.4c). The E-W speed fluctuates between 6 and –18 cm·s^{-1} while N-S

component values stay between 7 and –5 cm·s^{-1}. Periods of westward current intensification are observed at the end of March, end of April and mid May. The origin of those pulses is unknown. Two episodes of increased near bottom eddy-like activity have been previously recorded in the study area between July 97 and May 98 (Fabres et al., 2002). The second of these episodes partly overlaps with the period studied in the current paper, ending at the mid-May westward pulse.

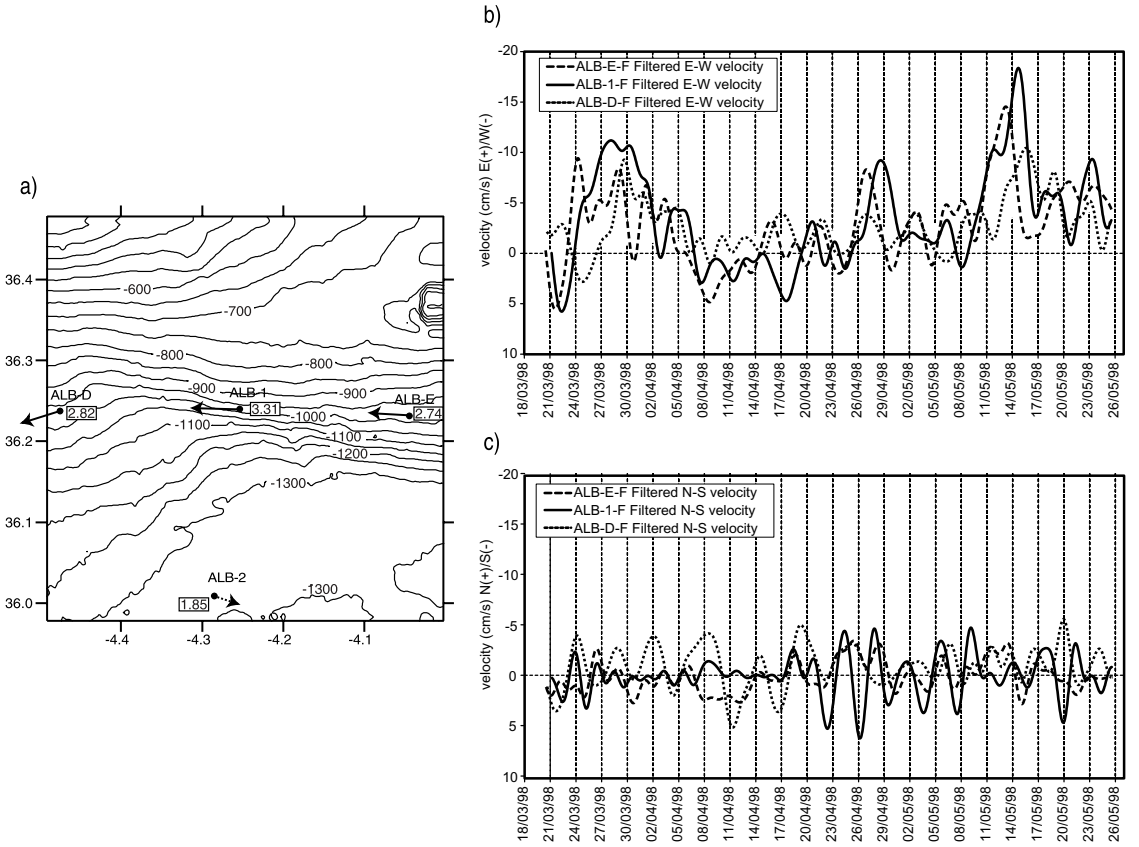

Figure 3.4. Bathymetric map (a) displaying the detailed seafloor morphology of the study area and the current residual vectors at ALB-E, ALB-1, ALB-D and ALB-2-S current meter locations. Temporal evolution of the E-W (b) and N-S (c) low pass-filtered components of the current at the three near bottom current meters of the mooring lines ALB-E, ALB-1 and ALB-D. The speed axes are inverted (negative values above and positive below) to facilitate later comparison with particulate fluxes.

3.4. Particle fluxes

3.4.1. Total mass flux

The temporal evolution of total mass fluxes (TMF) follows a common general trend in all stations and depths (Figs. 3.5-3.8). Two distinct periods can be identified. The first extends from the 1st of April until the end of the month or beginning of May, depending on the precise timing of each cup set. It is characterised either by low particle fluxes, as in the northern stations ALB-1, ALB-D and ALB-E (Figs. 3.5 and 3.8), or by a steady decrease from a high value to a minimum, as in ALB-2 (Fig. 3.6). During this period, TMF ranges from 200 to 500 mg·m^{-2}·day^{-1} in ALB-1-S surface trap, and between 500 and 1500

$mg \cdot m^{-2} \cdot day^{-1}$ at the bottom traps of the northern stations ALB-1-F, ALB-D-F and ALB-E-F. TMF decreases from 1000 to 200 $mg \cdot m^{-2} \cdot day^{-1}$ and from 1500 to 700 $mg \cdot m^{-2} \cdot day^{-1}$ in the surface and near bottom traps of the southern station ALB-2, respectively.

The second period, lasting from the end of April-beginning of May until the finalisation of the HFF experiment on May 22nd, coincides with a marked increase of TMF in all the stations and depths but ALB-2-I, where only a faint TMF increase was recorded. Even on the intermediate trap ALB-2-I the flux increase exceeds 100% with respect to the low values typical of the first period (Figs. 3.5 to 3.8). Such general increase peaks at different moments on different stations and depths. In the surface trap ALB-1-S two noticeable peaks were recorded centred on the 3rd and 9th of May (samples 7 and 9). The rising flank of a third peak is also observed from May 17th onwards (sample 12) (Fig. 3.5). Meanwhile, near bottom traps in all the northern stations ALB-D-F, ALB-1-F and ALB-E-F recorded two complete peaks centred on the 6th and 15th of May (samples 8 and 11) (Fig. 3.8). The southern mooring line recorded just one peak, which is centred on the 6th of May (sample 8) at intermediate depths (ALB-2-S and ALB-2-I traps) and on the 12th of May (sample 10) near the bottom (ALB-2-F) (Fig. 3.6).

The transition from the first to the second main period is not totally synchronous at all stations and depths. It was first recorded on the deep ALB-E-F trap on April 27th, followed by traps ALB-1-S, ALB-1-F, ALB-D-F and ALB-2-S on April 30th and, finally, by ALB-2-I and ALB-2-F traps on May 3rd (Figs. 3.7 and 3.8)

Trap code	TMF	Total C	Organic C (%)	Opal (%)	Org. matter (%)	$CaCO_3$ (%)	Lithogenic (%)
ALB-1-S	523.05	44.11 (8.43%)	36.03 (6.89%)	48.53 (9.28%)	72.06 (13.78%)	67.28 (12.86%)	335.19 (64.08%)
ALB-1-F	1100.51	66.14 (6.01%)	42.34 (3.85%)	66.78 (6.07%)	84.68 (7.69%)	198.27 (18.02%)	750.78 (68.22%)
ALB-E-F	1208.89	74.84 (6.19%)	49.36 (4.08%)	96.83 (8.01%)	98.71 (8.17%)	212.24 (17.56%)	801.10 (66.27%)
ALB-D-F	1472.03	83.82 (5.69%)	55.73 (3.79%)	92.81 (6.30%)	111.45 (7.57%)	234.00 (15.90%)	1033.76 (70.23%)
ALB-2-S	660.43	55.95 (8.47%)	45.33 (6.86%)	48.65 (7.37%)	90.66 (13.73%)	88.42 (13.39%)	432.70 (65.52%)
ALB-2-I	512.75	36.28 (7.08%)	27.80 (5.42%)	28.33 (5.52%)	55.60 (10.84%)	70.69 (13.79%)	358.13 (69.85%)
ALB-2-F	1187.92	68.26 (5.75%)	44.14 (3.72%)	61.50 (5.18%)	88.27 (7.43%)	200.96 (16.92%)	837.19 (70.48%)

Table 3.3. Total mass and main constituent time weighed fluxes (TWF, $mg \cdot m^{-2} \cdot day^{-1}$), also in percentages. The number of samples is 12 per trap, without exception.

The horizontal distribution of TMF is rather variable and it is thus difficult to draw spatial overall trends for particle fluxes. Comparison of the two upper traps at 400-500 m depth (Fig.3.7) reveals that, during the first of the periods described above, TMF is lower at the central northern station (ALB-1) than in the southern station (ALB-2). By contrast, during the second period the northern site shows TMF values that are most often higher than in the southern site for those upper traps. On average, TMF is slightly higher at the northern site (Table 3.3). For the four near bottom traps, higher TMF are observed in

the southern site ALB-2 during the first period, and in the northern sites ALB-1, ALB-D and ALB-E during the second period (Fig. 3.8). Within the three northern sites, TMF is on average highest at ALB-D-F and lowest at ALB-1-F (Table 3.3).

The depth distribution of particle fluxes illustrates a downward decrease at intermediate depths and a pronounced increase near bottom (Table 3.3). Time weighed flux (TWF) at station ALB-1 increases from 523 $mg \cdot m^{-2} \cdot day^{-1}$ at the trap located at 500 m depth, ALB-1-S, to 1100 $mg \cdot m^{-2} \cdot day^{-1}$ at 30 masf (m above sea floor), ALB-1-F. At ALB-2 values decrease from 660 to 513 $mg \cdot m^{-2} \cdot day^{-1}$ between the traps located at 400 m and 900 m depth, ALB-2-S and ALB-2-I, and increase up to 1188 $mg \cdot m^{-2} \cdot day^{-1}$ at the 30 masf trap, ALB-2-F.

3.4.2. Fluxes of major constituents

Time weighed percentages of major constituents for the whole set of traps are as follows: lithogenic fraction from 64% up to 70%, carbonate from 13% up to 18%, organic matter from 7% up to 14% and opal from 5% up to 9% (Table 3.3). This decreasing trend from lithogenics to opal is observed in all traps excepting the two traps located at 400-500 m depth, ALB-1-S and ALB-2-S, where organic matter is slightly more abundant than carbonate. The temporal series of the fluxes of major constituents are displayed on Figures 3.5 to 3.8 together with TMF time series. The temporal evolution of main constituent fluxes roughly follows the evolution of TMF at all stations and depths because of the high variability of TMF when compared to the moderate variability of the relative abundance of each constituent. Nevertheless, the variability in the contributions of mainly organic matter and opal versus carbonate and lithogenics highlights the differences between the two periods described above, roughly covering April and May, respectively.

Opal and organic matter fluxes seem to be much more independent from TMF than carbonate and lithogenics fluxes, despite being the least abundant constituents. Opal fluxes are typically below 50 $mg \cdot m^{-2} \cdot day^{-1}$ during the first period to peak up to three to six times higher during the second period. Opal abundance is usually below 5% during the first period and around 10-15% during the second period. The relative abundance of opal is lower and less fluctuating near bottom than at the intermediate depths, especially during high flux periods. However, this does not imply lower fluxes at depth, as is the case for ALB-1 station. All **organic matter** fluxes are below 100 $mg \cdot m^{-2} \cdot day^{-1}$ during the first period, while during the second period fluxes peak above 150 $mg \cdot m^{-2} \cdot day^{-1}$. Maximum organic matter relative abundance during the second period (14 to 24% for intermediate depths and 7 to 12% near bottom) almost doubles the values recorded during the first period (7 to 16% and 5 to 8% for intermediate depths and near bottom, respectively) (Figs. 3.7 and 3.8). As for opal, the relative abundance of organic matter near bottom (Fig. 3.8) is less fluctuating than at intermediate depths.

Carbonate relative abundance does not follow the two period pattern, although carbonate fluxes still follow it. Near bottom values (Fig. 3.8) are much less variable (from 13 to 23%) than intermediate

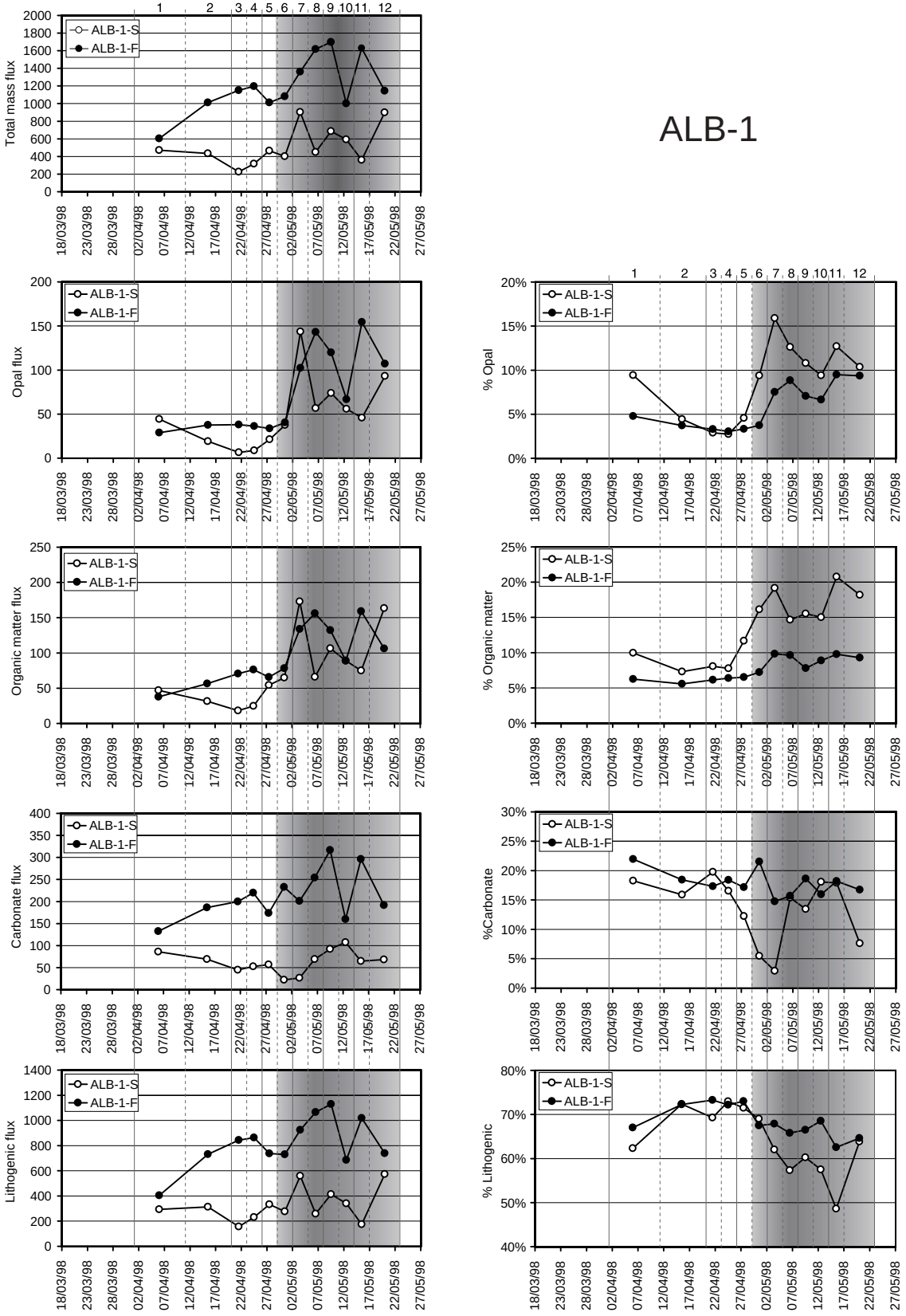

Figure 3.5. Temporal evolution of total mass fluxes ($mg \cdot m^{-2} \cdot d^{-1}$) and fluxes and percentages of main constituents for ALB-1 sediment traps. Numbers from 1 to 12 on the upper horizontal axis and associated vertical lines indicate the duration of the sampling for each of the 12 cups in every sediment trap. Dates are given in the lower horizontal axis. Greyed interval represents the second period described in the main text.

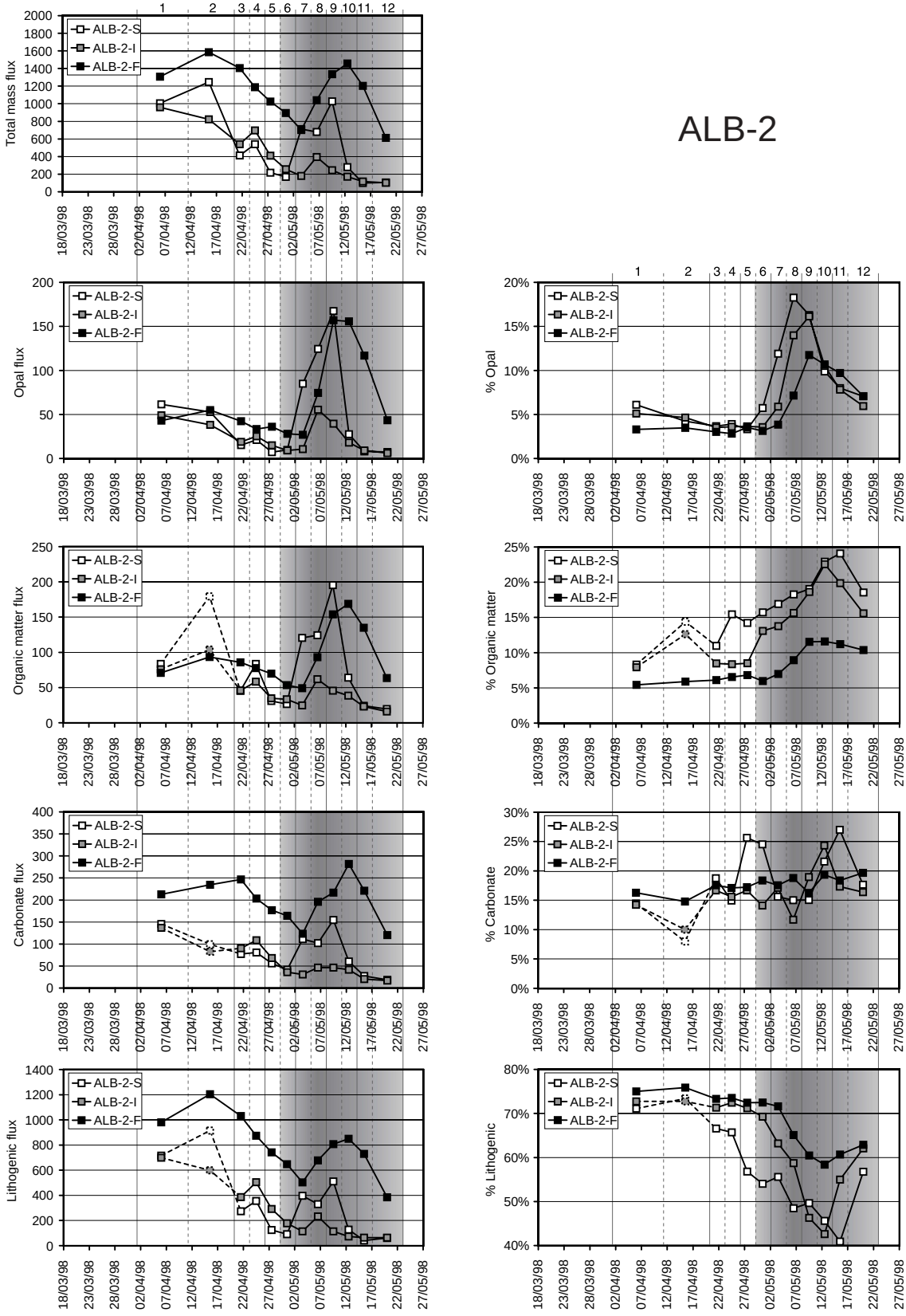

Figure 3.6. Temporal evolution of total mass fluxes ($mg \cdot m^{-2} \cdot d^{-1}$) and fluxes and percentages of main constituents for ALB-2 sediment traps. Dashed segments indicate values potentially affected by the presence fish remains on the samples. Numbers from 1 to 12 on the upper horizontal axis and associated vertical lines indicate the duration of the sampling for each of the 12 cups in every sediment trap. Dates are given in the lower horizontal axis. Greyed interval represents the second period described in the main text.

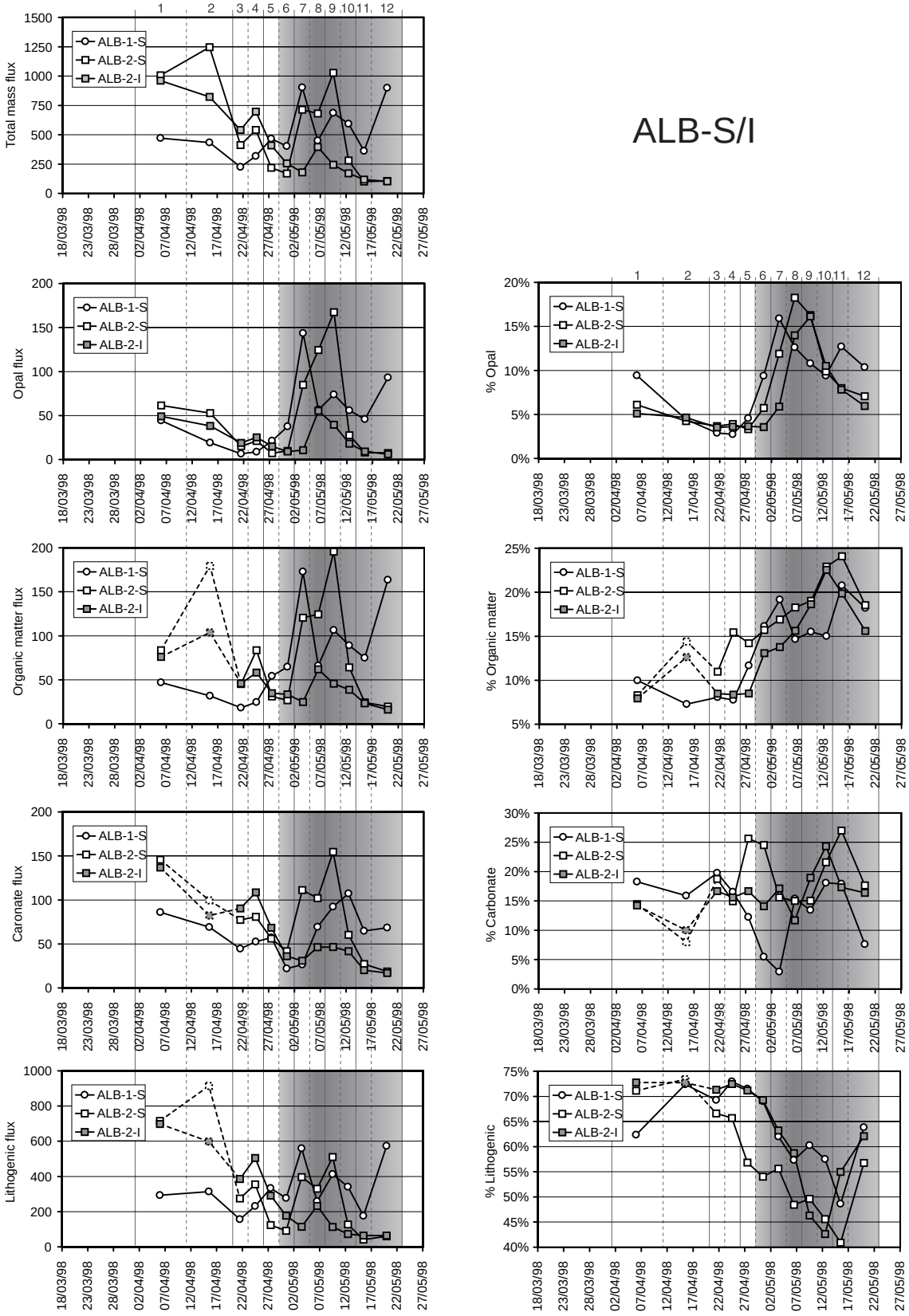

Figure 3.7. Temporal evolution of total mass fluxes ($mg \cdot m^{-2} \cdot d^{-1}$) and fluxes and percentages of main constituents for the shallow and intermediate sediment traps. Dashed segments indicate values potentially affected by the presence fish remains on the samples. Numbers from 1 to 12 on the upper horizontal axis and associated vertical lines indicate the duration of the sampling for each of the 12 cups in every sediment trap. Dates are given in the lower horizontal axis. Greyed interval represents the second period described in the main text.

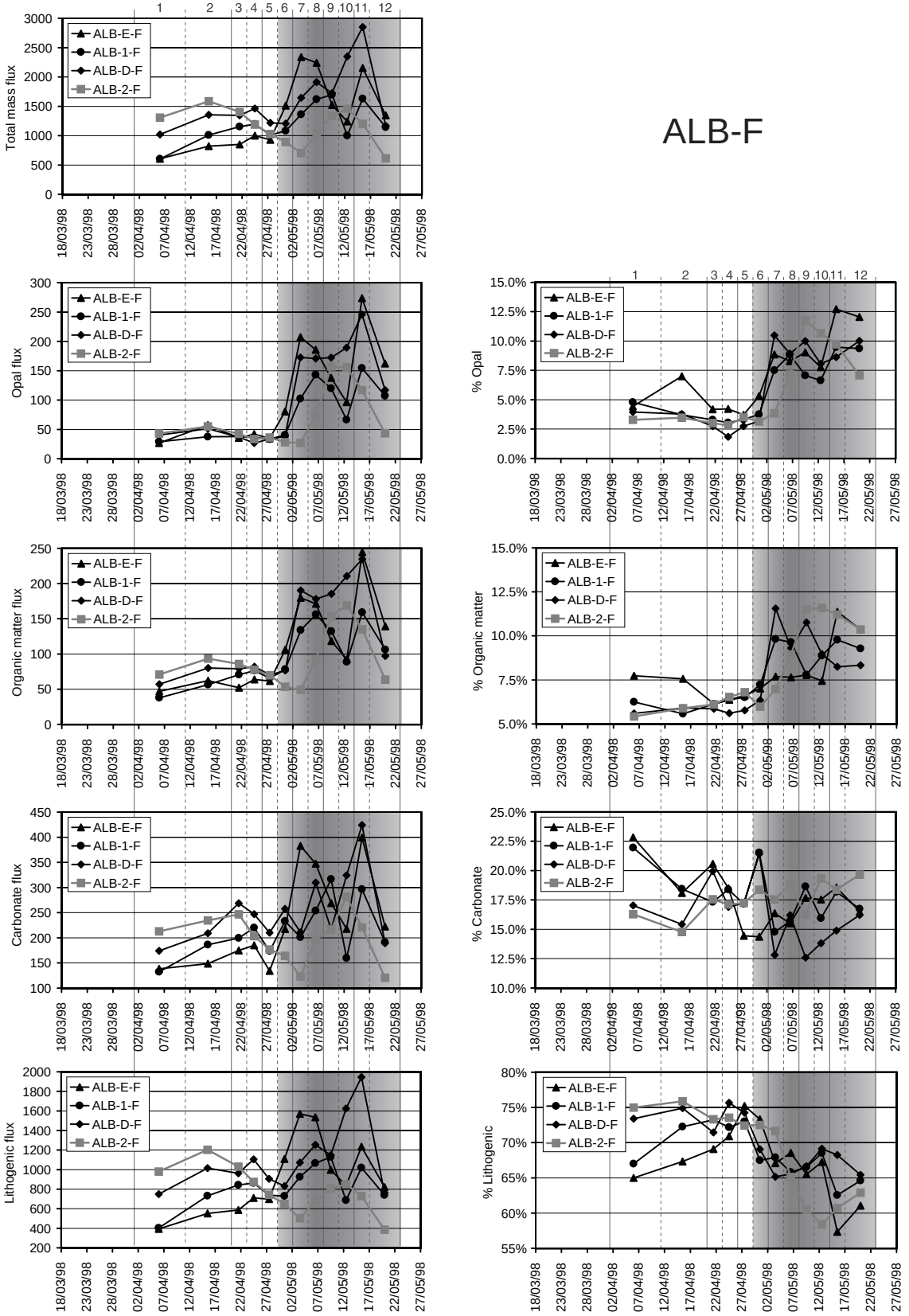

Figure 3.8. Temporal evolution of total mass fluxes ($mg \cdot m^{-2} \cdot d^{-1}$) and fluxes and percentages of main constituents for the sediment traps located at 30 metres above the sea floor. Numbers from 1 to 12 on the upper horizontal axis and associated vertical lines indicate the duration of the sampling for each of the 12 cups in every sediment trap. Dates are given in the lower horizontal axis. Greyed interval represents the second period described in the main text.

water values (from 3 to 27%) (Fig. 3.7). Carbonate fluxes near bottom (Fig. 3.8) range between 132 and 267 $mg \cdot m^{-2} \cdot day^{-1}$ during the first period and between 120 and 424 $mg \cdot m^{-2} \cdot day^{-1}$ during the second one. Intermediate depth fluxes (Fig.3.7) range between 17 and 155 $mg \cdot m^{-2} \cdot day^{-1}$ in both periods.

The lithogenic fraction follows the two period pattern inversely, if compared to organic matter and opal. Therefore, high relative abundance appears during the first period, usually around 70%, while minimum relative abundance is observed during the second period, with values lower than 50% at intermediate depths and lower than 60% near bottom (Figs. 3.7 and 3.8). In the southern station, the inverse behaviour of the lithogenic fraction relative abundance jointly with the high TMF values at the beginning of the first period imply higher maximum lithogenic fluxes (from 716 to 1203 $mg \cdot m^{-2} \cdot day^{-1}$) than those recorded (from 232 to 850 $mg \cdot m^{-2} \cdot day^{-1}$) during the second period (Figs 3.7 and 3.8). Such a tendency is less pronounced in the northern stations, thus generating maximum lithogenic fluxes to be higher during the second period (from 573 to 1945 $mg \cdot m^{-2} \cdot day^{-1}$ depending on the trap) than during the first period (from 333 to 1106 $mg \cdot m^{-2} \cdot day^{-1}$). Lithogenic fluxes are significantly higher near bottom than at intermediate depths (Figs. 3.5 and 3.6), in accordance with the carbonate pattern.

3.4.3. Ratios of major biogenic elements

The ratios between the major biogenic elements (C, N and Si) summarise the compositional characteristics of the trapped particle population. These ratios represent a valuable source of essential information about autochthonous particles since they are less affected than the percentages and fluxes of main constituents by the variable dilution by allochthonous (mainly lithogenic) particles. Moreover, Si and N play a key role as major nutrients in regulating primary production and, therefore, the entire water column ecosystem. This is particularly the case if diatoms are part of the phytoplankton association as it occurs in coastal upwellings. The differences in the cycles of these two elements in surface waters support the use of Si/N ratios as a way of tracking the trophic pathways followed by particles during their export to deeper waters. While nitrogen is retained in the trophic chain, i.e. in the tissues grazing zooplankton, Si is exported as SiO_2 to be recycled only by dissolution in deeper waters. This results in an augmentation of Si/N ratios when a high proportion of the particles exported from surface waters have been reprocessed by grazing zooplankton (Dugdale et al., 1995).

Time series of Si/N, Si/C and C/N are presented grouped by mooring lines (ALB-1 and ALB-2) on Figure 3.9, and according to trap water depths (intermediate, ALB-S/I, and near bottom, ALB-F) on Figure 3.10. Si/N values fluctuate between 0.5 and 3 at intermediate depths and between 1 and 4 near the bottom. The two-period evolution described for major constituents in Section 3.4.1 is observed also in the Si/N ratio. While at intermediate depths the first period shows decreasing values through time, a gradual increase appears between the end of April and the beginning of May followed by a new decrease towards the end of the second period. This evolution is not completely synchronous for the three mid-water stations, occurring first at ALB-1-S and last at ALB-2-I. Both the increase and the decrease are more gradual on ALB-1-S than at the other two stations. The evolution of the Si/N ratio near the bottom is

clearly divided into two different periods also, the first with lower values, mostly between 1 and 2.5, and the second with higher values, mostly between 2.5 and 4. The shift between the two is rather dramatic as it occurs drastically between two consecutive samples, excepting in ALB-E-F where the change is more gradual.

Si/C evolution parallels that of Si/N with values that fluctuate between 0.08 and 0.36 at intermediate depths and between 0.12 and 0.43 near the bottom (Fig. 3.10). Finally, C/N values range from 6 to 10 at intermediate depths, and from 8 to 10 near the bottom. C/N values at intermediate depths fluctuate strongly during the first period and become much more homogeneous during the second period. Such a relative homogeneity is maintained during the whole experiment near the bottom (Fig. 3.10).

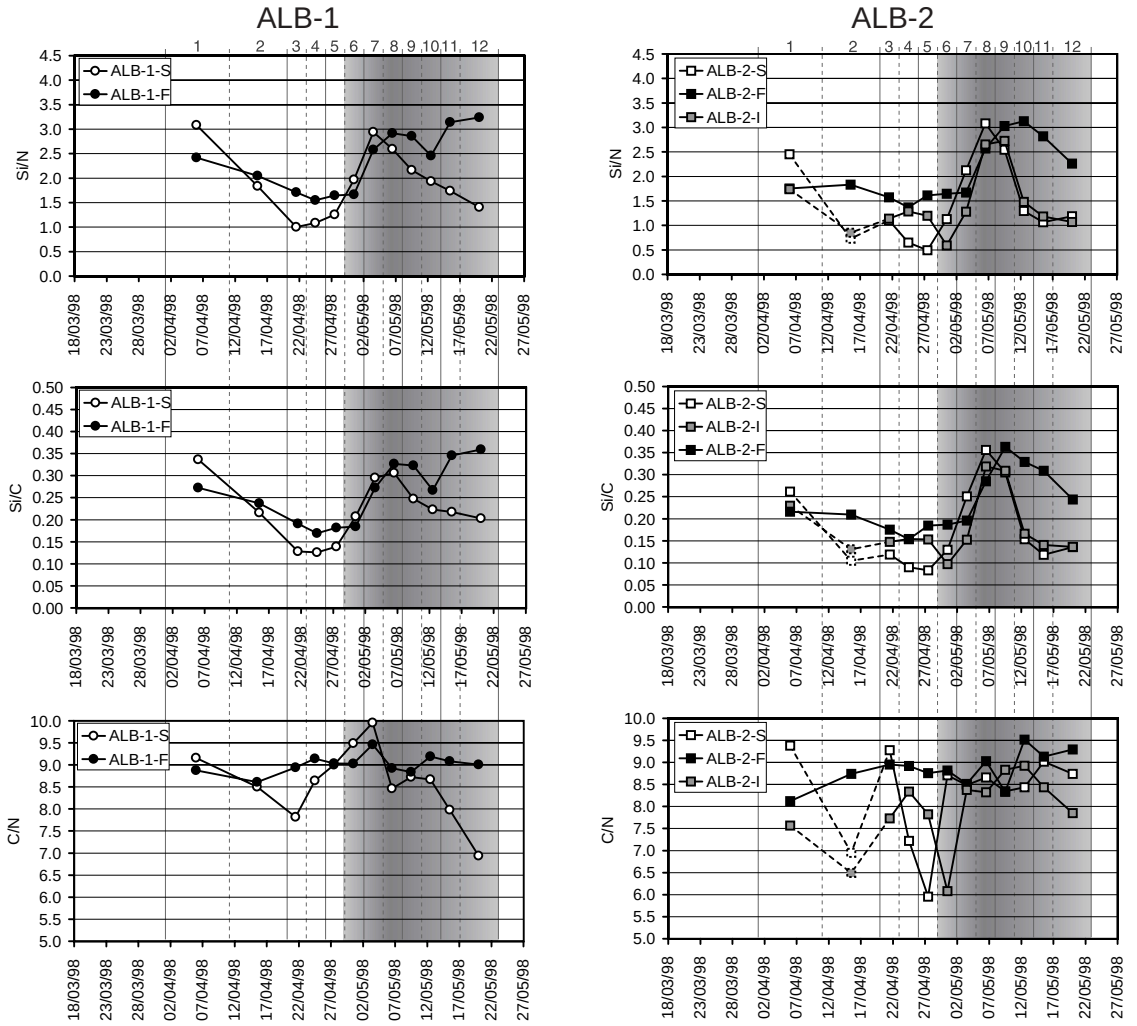

Figure 3.9. Si/N, Si/C and C/N atomic ratios for traps belonging to moorings ALB-1 and ALB-2. Greyed interval represents the second period described in the main text.

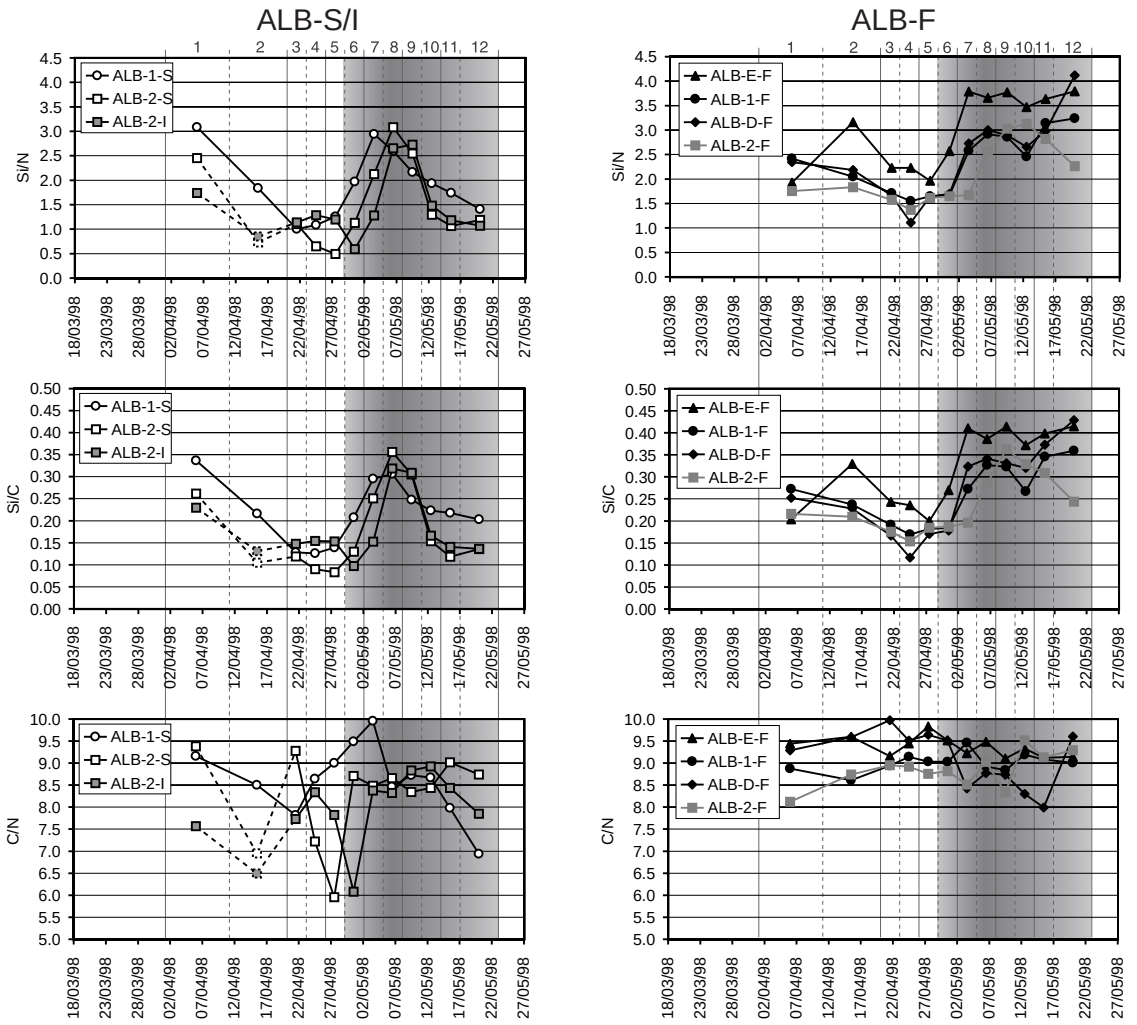

Figure 3.10. Si/N, Si/C and C/N atomic ratios for traps located at intermediate depths (ALB-S/I) and traps located near the bottom (ALB-F). Greyed interval represents the second period described in the main text.

3.5. Discussion

3.5.1. Particle vertical settling speed

Calculation of particle settling velocities allows to determine when particles collected were exported from the photic zone and started their descent into the water column. Direct comparison between particle flux time series and sea surface data using the calculated transfer times is used to determine the conditions triggering particle production and export from surface waters.

The pair of traps that allows vertical particle settling speed calculations is ALB-2-S/ALB-2-I. The remaining pairs located at the same station (ALB-1-S/ALB-1-F and ALB-2-I/ALB-2-F) are not suitable for particle settling speed calculation as higher TWF and 3-day flux values near the bottom (Figs. 3.5 and 3.6) indicate lateral advective input of particulate material. This near bottom advective input has

been highlighted in former works in the WAB (Fabres et al., 2002; Masqué et al., in press) and is discussed in detail in Section 3.5.4.

In the ALB-2-S/ALB-2-I pair there is a flux peak from the end of April to mid May that can be perfectly delimited with various markers in both traps. This flux peak has a distinct signature in TMF but also in opal (flux and percentage), organic matter, carbonate (Fig. 3.7) and, specially, Si/N and Si/C ratios (Fig. 3.10). The flux peak at ALB-2-I is, however, much lower than at ALB-2-S suggesting sequestration and/or degradation of the particulate material between 400 and 900 m of water depth. This point is further discussed below.

Berelson (2002) has studied particle settling rates using flux ratios between biogenic elements in order to overcome the problems derived from partial transfer of particles between two depths and the inaccuracy of particle flux data gathered from sediment traps. We have followed his approach which assumes that (i) there are temporal variations in the elemental ratios of settling material, (ii) particles follow a vertical trajectory during settling below the surface layer and, (iii) that settling speed does not change as a function of depth. We consider, in addition, and as a first approximation, that all the particles trapped in the same cup have the same settling speed and that the elemental ratios of the material exported from the surface layer change linearly with time. Si/N and Si/C ratios are the best markers for calculating settling speeds in the WAB since, first, they show the highest coherence and, second, the maximum and minimum values are very close in both traps, thus indicating that none of the two ratios is significantly affected by microbial remineralization during particle settling in the water column.

This approach allows calculation of average transfer times for particles collected in cups with homogeneous time intervals (3 days) as sinking from ALB-2-S down to ALB-2-I. For this we determine by linear interpolation the date (transfer date in Table 3.4) at which the material at ALB-2-I would have the same elemental ratio as the material collected formerly in the shallower ALB-2-S trap (see Fig. 3.11 and Table 3.4). Once the transfer date is known, the transfer time and settling speed between both traps can be calculated. The settling speed is then used to calculate by extrapolation the time needed by particles to sink from 100 m (bottom of surface layer) to ALB-2-S depth (100-400 m transfer time in Table 3.4). Finally, the theoretical time range during which particles collected within a given sample of the ALB-2-S trap were exported from the 100 m surface layer is calculated by subtracting the transfer time of the opening and closing dates for that sample.

As it can be observed in Table 3.4 settling speeds calculated from Si/N data differ from those calculated from Si/C data but the ranges for each sample are similar excepting on the highest speed range. Highest settling speeds calculated by this method have to be regarded cautiously as small errors in the chemical analysis and the uncertainty due to step sampling of sediment traps can lead to significant changes of several hundreds or even thousands of meters per day. That may be the case for the extremely high settling speed calculated for sample 9 using Si/C ratios. Apart from that one the rest of calculated settling speeds fall well within the settling speed range cited in the literature for natural particles settling in marine waters (i.e. Alldredge and Gotshalk, 1989; Bory et al., 2001). Settling speeds reported in Table 3.4 fluctuate between 80 and more than 300 $m \cdot d^{-1}$, implying that the particles were exported from the surface 100 m layer between four and less than one day before being captured in ALB-2-S trap. When

using those transfer times to track back which time periods are represented in each cup (last two columns of Table 3.4) we realise that, there were time periods that were theoretically not represented in any cup or periods represented in two of them. That is the result of considering that all particles trapped in the same cup have the same settling speed leading to a step-like evolution in settling speed and transfer times. Nevertheless the information obtained from this analysis is still a good tool to infer approximately when the particles collected at intermediate depths left the surface photic layer.

As it can be observed in Table 3.4 settling speeds calculated from Si/N data differ from those calculated from Si/C data but the ranges for each sample are similar excepting on the highest speed range. Highest settling speeds calculated by this method have to be regarded cautiously as small errors in the chemical analysis and the uncertainty due to step sampling of sediment traps can lead to significant changes of several hundreds or even thousands of meters per day. That may be the case for the extremely high settling speed calculated for sample 9 using Si/C ratios. Apart from the later the calculated settling speeds fall well within the settling speed range cited in the literature for natural particles settling in marine waters (i.e. Alldredge and Gotshalk, 1989; Bory et al., 2001). Settling speeds reported in Table 3.4 fluctuate between 80 and more than 300 $m \cdot d^{-1}$, implying that the particles were exported from the surface 100 m layer between four and less than one day before being captured in ALB-2-S trap. When using those transfer times to track back which time intervals are represented in each cup (last two columns of Table 3.4) we realise that some are theoretically not represented in any cup while others are represented in two consecutive cups. This results from considering that all particles trapped in the same cup have the same settling speed, thus leading to a step-like evolution in settling speed and transfer times. Even with the cautions above, this analysis is still a good tool to infer approximately when the particles collected at intermediate depths left the surface photic layer.

Although settling speed calculation cannot be done for particles collected at ALB-1-S due to the lack of an intermediate trap devoid of near bottom advective influence, a rough estimate of settling speeds can be carried out for the period from the end of April to the beginning of May assuming that particles with similar elemental ratios and composition have similar settling rates. Consequently, as Si/N and Si/C evolution of samples 5 to 8 in ALB-1-S parallels that of samples 6 to 9 in ALB-2-S (Fig. 3.9), we can estimate that particles collected in samples 5 and 6 in ALB-1-S had an average settling speed of around 200-300 $m \cdot d^{-1}$ while those collected in samples 7 and 8 had settling speeds well above 300 $m \cdot d^{-1}$. This resulted in transfer times (between ~100 m and ~500 m depth) of one or two days for samples 5 and 6 and less than one day for samples 7 and 8. Hence, disregarding the difference in trap depths, transfer times are almost the same for synchronous samples at both traps so they represent almost the same export periods from surface layer.

Settling speeds reported here are substantially higher than those reported previously (> 50 $m \cdot d^{-1}$) in the WAB from lower resolution flux data (Fabres et al., 2002). This is because higher sampling resolution allows resolving higher settling speeds, and also because former estimations were based on comparisons between particle flux and river discharge or surface chlorophyll time series instead of parallel flux time series. Surface data sets, apart from having lower temporal resolution (especially for

	OPENING DATE	CLOSING DATE	SAMPLING TIME (days)	MIDPOINT DATE	Si/N ALB-2-S	Si/N ALB-2-I	TRANSFER DATE	400-900 m TRANSFER TIME (days)	**SETTLING SPEED ($m \cdot d^{-1}$)**	**100-400 m TRANSFER TIME (days)**	SURFACE (100 m) TRANSFER START	SURFACE (100 m) TRANSFER END
1	1/4/98 00	11/4/98 00	10	6/4/98 00	2.45	1.74						
2	11/4/98 00	20/4/98 00	9	15/4/98 12	0.73	0.85						
3	20/4/98 00	23/4/98 00	3	21/4/98 12	1.11	1.14	26/4/98 10	6.5	**77**	**3.9**	16/4/98 03	19/4/98 03
4	23/4/98 00	26/4/98 00	3	24/4/98 12	0.65	1.28	28/4/98 16	5.7	**88**	**3.4**	19/4/98 13	22/4/98 13
5	26/4/98 00	29/4/98 00	3	27/4/98 12	0.50	1.20	29/4/98 11	3.5	**144**	**2.1**	23/4/98 22	26/4/98 22
6	29/4/98 00	2/5/98 00	3	30/4/98 12	1.13	0.59	1/5/98 08	2.4	**212**	**1.4**	27/4/98 14	30/4/98 14
7	2/5/98 00	5/5/98 00	3	3/5/98 12	2.13	1.28	3/5/98 20	1.9	**270**	**1.1**	30/4/98 21	3/5/98 21
8	5/5/98 00	8/5/98 00	3	6/5/98 12	3.08	2.65	5/5/98 22	0.9	**532**	**0.6**	4/5/98 10	7/5/98 10
9	8/5/98 00	11/5/98 00	3	9/5/98 12	2.55	2.73	8/5/98 10	0.4	**1147**	**0.3**	7/5/98 17	10/5/98 17
10	11/5/98 00	14/5/98 00	3	12/5/98 12	1.30	1.48	12/5/98 21	1.9	**266**	**1.1**	9/5/98 20	12/5/98 20
11	14/5/98 00	17/5/98 00	3	15/5/98 12	1.07	1.18						
12	17/5/98 00	23/5/98 00	6	20/5/98 00	1.19	1.07						

	OPENING DATE	CLOSING DATE	SAMPLING TIME (days)	MIDPOINT DATE	Si/C ALB-2-S	Si/C ALB-2-I	TRANSFER DATE	400-900 m TRANSFER TIME (days)	**SETTLING SPEED ($m \cdot d^{-1}$)**	**100-400 m TRANSFER TIME (days)**	SURFACE (100 m) TRANSFER START	SURFACE (100 m) TRANSFER END
1	1/4/98 00	11/4/98 00	10	6/4/98 00	0.26	0.23						
2	11/4/98 00	20/4/98 00	9	15/4/98 12	0.10	0.13						
3	20/4/98 00	23/4/98 00	3	21/4/98 12	0.12	0.15	29/04/98 07	7.8	**64**	**4.7**	15/4/98 07	18/4/98 07
4	23/4/98 00	26/4/98 00	3	24/4/98 12	0.09	0.15	30/04/98 20	6.4	**79**	**3.8**	19/4/98 04	22/4/98 04
5	26/4/98 00	29/4/98 00	3	27/4/98 12	0.08	0.15	01/05/98 05	3.7	**134**	**2.2**	23/4/98 18	26/4/98 18
6	29/4/98 00	2/5/98 00	3	30/4/98 12	0.13	0.10	02/05/98 06	1.8	**282**	**1.1**	27/4/98 22	30/4/98 22
7	2/5/98 00	5/5/98 00	3	3/5/98 12	0.25	0.15	05/05/98 06	1.8	**282**	**1.1**	30/4/98 22	3/5/98 22
8	5/5/98 00	8/5/98 00	3	6/5/98 12	0.36	0.32	07/05/98 04	0.7	**743**	**0.4**	4/5/98 14	7/5/98 14
9	8/5/98 00	11/5/98 00	3	9/5/98 12	0.30	0.31	09/05/98 13	0.1	***6330***	***0.0***	7/5/98 22	10/5/98 22
10	11/5/98 00	14/5/98 00	3	12/5/98 12	0.15	0.17	13/05/98 22	1.5	**343**	**0.9**	10/5/98 03	13/5/98 03
11	14/5/98 00	17/5/98 00	3	15/5/98 12	0.12	0.14						
12	17/5/98 00	23/5/98 00	6	20/5/98 00	0.14	0.14						

Table 3.4. Particle settling speed calculation through the use of Si/N and Si/C ratios. All the dates are in the dd/mm/yy hh format.

chlorophyll), essentially mark the time when particles enter the system and not necessarily the time when they start their descent towards the bottom.

Further implications of the evolution of particle flux composition, element ratios and settling rates of the particles collected during the second period covering the month of May will be discussed altogether with SST, chlorophyll-a concentration in surface waters and hydrographic structure data in the following section.

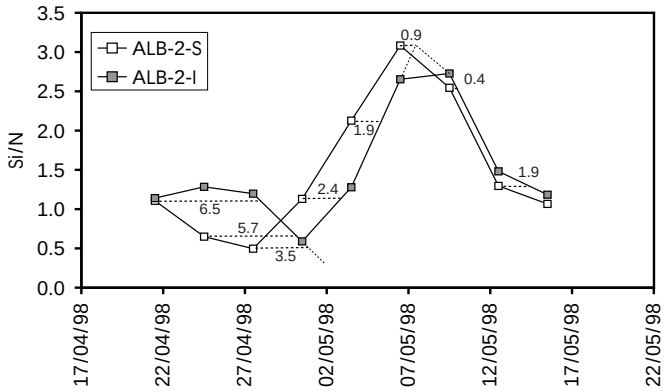

Figure 3.11. Ilustration of the method used for particle settling speed calculation based in atomic Si/N ratios. Numbers in the graph correspond to the estimated time (in days) needed by the particles collected in ALB-2-S (400 m) to reach the depth of ALB-2-I (900 m) trap.

3.5.2. Particle flux export from surface waters

Since during spring 1998 the supply of riverine-born particles was greatly reduced (Fabres et al., 2002), flux spatio-temporal variability may have been controlled mostly by biologically-mediated processes in the surface layers (i.e. particle production and aggregation) and export-transfer mechanisms affecting this particulate matter.

Particle flux evolution during the HFF experiment is divided in the two periods mentioned above. The first period is characterised by the paucity of particle fluxes with the only exception of the high fluxes dominated by the lithogenic and the carbonate fractions at the beginning of the period on ALB-2 station. Both ALB-2-S and ALB-2-I organic matter time series have a flux peak corresponding to the second cup that is not paralleled by any other biogenic component. This peak results from high total mass fluxes combined with high organic matter abundance likely caused by contamination of the particulate material due to the capture of fishes within the cup (cf. Section 3.2.2). Low C/N values, though not excluding other origins may be caused by the contamination with protein rich fish remains. Figures potentially affected by this kind of contamination are displayed with dashed lines in Figures 3.5 to 3.10.

The most conspicuous flux events are recorded during the second period from the end of April onwards. The higher resolution of our flux record and the better temporal coverage of SeaWiFS and SST

images allow to discern the first order factors controlling particle export to intermediate and deep waters. In general, this second period is characterised by temporally and spatially variable high particle fluxes including a substantial contribution of organic matter and opal. Overall, three phases, named increasing, maximum and decreasing, can be distinguished within this period.

The **increasing phase**, which was recorded slightly earlier in ALB-1 (26/04-01/05) than in ALB-2 (29/04-04/05), is marked by the rise in organic carbon and opal percentages (Fig. 3.7), and in Si/N and Si/C ratios (Fig. 3.10). The latter move from 1 to 2 and from 0.1 to 0.25, respectively, for the two moorings. Si/N and Si/C ratios around 1 and 0.1 are typical of diatoms in temperate waters (Brzezinski, 1985). Therefore, settling of diatom aggregates scavenging abundant lithogenic particles seems the most likely origin for the particles collected at the beginning of this phase. The subsequent progressive increase in Si/N and Si/C could reflect the onset of zooplankton grazing on the phytoplanktonic community. Dugdale et al. (1995) predicted Si/N ratios between 2 and 3 for material consisting of a mixture of faecal pellets and diatom cells exported from an upwelling area with low to moderate zooplankton grazing.

It is to be noted that before the beginning of the increasing phase, during the first period, Si/N and Si/C values even lower than those reported above were recorded. This likely indicates that the little biogenic material settling down at that time was mainly composed of non-silica phytoplankton which is typical of oligotrophic conditions in the Alboran Sea (Claustre et al., 1994). The enhancement of zooplankton grazing may have triggered an increase in faecal pellet production and consequently the increase in organic carbon and opal fluxes recorded along this phase. Settling speed augmentation, from ~150 $m \cdot d^{-1}$ before the beginning of the increasing phase to 200-300 $m \cdot d^{-1}$ through it (Table 3.4), is probably caused by the change in the composition of settling material and zooplankton-mediated aggregation. These speeds are in the higher range of the speeds cited by Takahashi (1986) and Alldredge and Gotschalk (1989) for diatom aggregates suggesting that faecal pellet production contributed fast settling particles to the flux.

As discussed in Section 3.5.1, particles collected during the increasing phase may have left the surface layer between 24/04 and 30/04 for ALB-1-S, and between 27/04 and 03/05 for ALB-2-S. SeaWiFS images along these time spans show that the productive margin of the gyre approached the position of ALB-1 station on 27/04 (Fig. 3.2d) and that slightly chlorophyll-enriched waters recirculating from the southern edge of the WAG invaded its centre over the position of ALB-2 towards the end of this phase (Fig. 3.2e). This situation explains the minimum fluxes recorded during the days preceding the second period increasing phase and the delayed onset of biogenic-enriched particle fluxes in the centre of the gyre (ALB-2) with respect to its northern edge (ALB-1). The delayed augmentation of biogenic-rich particle fluxes with respect to the onset of upwelling-related productivity (around mid April) reflects that, as noticed by Ducklow et al. (2001), increased primary productivity does not always imply immediately enhanced fluxes. For such an enhancement to occur, transfer mechanisms, as zooplankton grazing, must be at work and this usually happens with a slight delay.

The **maximum phase** is characterised in ALB-1-S by a very sharp peak centred on days 02/05 to 04/05 followed by a decrease and then a second, lower peak centred on days 08/05 to 10/05. The evolution is slightly different in ALB-2-S, where the sharp increase from days 02/05 to 04/05 leads to a

deceleration preceding a second sharp increase that peaks on days 08/05 to 10/05. Opal percentages, Si/N and Si/C ratios record a similar evolution, reaching their maxima synchronously or slightly earlier than mass fluxes (Figs. 3.7 and 3.10). Particles collected during this phase had been exported from the surface layer approximately between 02/05 and 09/05 above ALB-1-S, and between 04/05 and 10/05 above ALB-2-S (Table 3.4). SST and SeaWiFS images from 04/05 to 06/05 (Figs 3.2g and 3.2h) illustrate the development of anticyclonic eddies associated to the northern edge of the WAG which advect phytoplankton-rich water masses from the periphery towards the centre of the gyre. Hydrographic sections of days 06/05 and 10-11/05 (Fig. 3.3) show several significant instabilities developed below these eddies on the upwelling tilted interface separating MAW and LIW. Particle and chlorophyll-laden water bodies subducting along isopycnals are associated to these small-scale instabilities on the MAW/LIW interface. In fact, the passage of small anticyclonic eddies probably induced the shearing and downwelling advection of phytoplankton-laden water bodies from the periphery towards the centre of the gyre.

Chlorophyll and phytoplankton composition supports such an advection mechanism as shown by the data collected by Arin et al. (2002) during the MATER-98 cruise. Their Chl-a > 20 µm data clearly indicate the N-S progression of a microplankton-dominated community below 60 m depth (see Fig. 6 in Arin et al., 2002). This community was detected at station A (see location on Figure 3.1) on day 02/05, at station B (above ALB-1) on day 03/05, and at station C (above ALB-2) from day 04/05 until at least day 07/05. Microscopy analysis of water samples taken at station C on 07/05 at 60, 80 and 100 m depth showed that this microplankton community was dominated by large diatoms which contributed with up to 84% of the carbon biomass in the 100 m surface layer, reaching values of 45 µg $C \cdot l^{-1}$ (see Fig. 7 in Arin et al., 2002).

The phytoplankton of a second Chl-a > 20 µm peak detected in station A between 40 and 60 m depth from 08/05 to 11/05 consisted of mainly diatoms, attaining up to 64% of the autotrophic biomass that reached values up to 75 $\mu g \cdot l^{-1}$. This peak matches the fluorescence maximum recorded at the same depth and station in the 10-11/05 hydrographic section (Fig. 3.3), which spread as far as the ALB-1 latitude below 100 m depth.

The overlap between surface export maxima, as indicated by fluxes recorded in ALB-1-S and ALB-2-S, and the progressive arrival to the subsurface of phytoplankton-enriched water bodies shows that particle fluxes are controlled by the passage of small anticyclonic gyres and by the isopycnal advection of diatom-rich water bodies. Variability is higher at ALB-1-S than at ALB-2-S because phytoplankton-rich water bodies just drift over the first of these stations while they remain, at least for some days, over the second one. Also, the persistency of higher particle fluxes in ALB-2-S is likely related to its location near the centre of the gyre, a place where large amounts of particles concentrate on subsurface waters thanks to the regular arrival of phytoplankton-enriched water bodies. The light transmission section of day 06/05 (Fig. 3.3) clearly illustrates such a higher concentration in the subsurface waters from the centre of the gyre, which behaves as a natural trap for particles. The focussing of particles towards the centre of the gyre has been already proposed in our former work (Fabres et al., 2002) but the precise mechanisms for enhanced fluxes were not resolved yet. Similarly, Peinert and

Miquel (1994), and Gorsky et al. (2002) report the impact of isopycnal downwelling on particle fluxes and large particulate matter distribution along the Almeria-Oran Front.

Aggregation processes are known to play a determinant role in triggering particulate fluxes from surface waters. The increase in particle concentration, as it may occur along the front and at the centre of the gyre, favours coagulation by increasing particle impact probability (Alldredge and Silver, 1988; Kiørboe, 2001). In addition to physical aggregation by coagulation, zooplankton mediated aggregation may have played a prime role in producing large aggregates that settle fast, thus contributing to flux maxima. Si/N and Si/C ratios reach about 3 and 0.3, respectively, in the material collected during the maximum phase. This highlights that grazing pressure and uptake of C and N by zooplankton attained moderate levels (Dugdale et al., 1995). Visual inspection of ALB-1-S and ALB-2-S trap samples showed abundant appendicularian houses from samples yielding maximum Si/N and Si/C values onwards. Besides, high numbers of salps where collected on zooplankton trawls over stations ALB-1 and ALB-2 during the MATER-98 cruise (F. Pagès, unpublished data). These two zooplanktonic microphagous groups are known to play a significant role in processing and packaging micro-, nano- and picoplankton, and even bacteria which are then transferred to pelagic depths through faecal pellets and discarded houses and mucus (Fortier et al., 1994). Hansen et al. (1996) have shown the potential of the appendicularian *Oikopleura dioica*, a species found in high numbers in the upper 200 metres of the Western Alboran Sea (Vives et al., 1975), in driving particulate fluxes during a spring phytoplankton bloom in the west coast of North-America. Both appendicularians and salps are known to have the ability to swarm and take advantage of event-scale episodes of increased resource availability as it would be the case of the advection of phytoplankton-rich water masses to subsurface depths.

The ability to track the speed of settling particles during an individual event allows relating the grazing activity maximum influence with the increase from < 300 $m \cdot d^{-1}$ to velocities well above this figure (Table 3.4). Sinking rates of discarded houses and *Oikopleura dioica* free faecal pellets are about 150 $m \cdot d^{-1}$ while salp pellets are known to have sinking rates up to 2700 $m \cdot d^{-1}$ (Fortier et al., 1994; Hansen et al., 1996). This outlines that strong settling velocity increases and, therefore, downward flux peaks are mostly related to the contribution of salp pellets and to the massive aggregation of the biogenic and lithogenic particles than to the transfer of free settling appendicularian houses and pellets.

The **decreasing** phase, from 11/05 till 22/05 (end of the recording period), is marked by a general diminution of fluxes and elemental ratios in both stations. The only exception is the last sample in ALB-1-S, which shows a noticeable flux rise not followed by elemental ratios (Figs. 3.7 and 3.10). The inability to calculate particle settling speeds in ALB-2-S from sample 10 onwards (Table 3.4) due to the variations in the sampling frequency, hinders a precise determination of the particle export periods represented by each sample. Notwithstanding the speed decrease, back to 200-300 $m \cdot d^{-1}$, recorded on the sample collected between 11/05 and 14/05 in ALB-2-S indicates that particles collected during this decreasing phase were exported from 10/05 onwards.

Mid May SST and SeaWiFS images show WAG having recovered its “normal” configuration with moderately productive filaments associated to the gyre edge (Fig. 3.2i). The image from day 07/05 (not shown) and the 10-11/05 hydrographic section (Fig. 3.3) illustrate that the small eddies had almost

vanished and that they were not so deep at the end of the former phase to completely disappear during the decreasing phase. Nevertheless, on day 16/05 a cold, chlorophyll-rich water mass upwelled near the coast, east of Gibraltar Strait started drifting to the north of the study area (Fig. 3.2i and 3.2j).

The slow down of the eddy activity limited the amount of particles able to reach the positions of ALB-1, where fluxes decreased progressively, and ALB-2, where the decrease was much sharper. ALB-1 station remained under the influence of the weekly productive filaments associated to the border of the gyre during the first part of this decreasing phase. In addition, ALB-1 was probably influenced by the chlorophyll-rich water mass that burst from Gibraltar Strait on 16/05. This water mass likely nourished surface waters with the biogenic and lithogenic particles collected in the last ALB-1-S sample. Besides reduced surficial productivity and particle arrival, the sharp diminution of the settling speed between the maximum and the decreasing phases in ALB-2-S also contributed to the sharp flux reduction.

Si/N and Si/C ratios decreased progressively and sharply in ALB-1-S and ALB-2-S, respectively (Fig. 3.10). This would indicate a lowering of the grazing pressure over the phytoplanktonic association. ALB-1-S values still indicate some influence of zooplankton grazing in the sample where the last increase was recorded, but such an influence was much lower than during the maximum phase. ALB-2-S ratios decrease suddenly, after the maximum phase, to values typical of temperate water diatoms which implies a drastic reduction in the grazing activity.

During this decreasing phase organic matter and lithogenic fraction abundances reach absolute maximum and minimum values, respectively (Fig. 3.7). This is probably the result of two factors combined. First, the massive physically- and biologically-mediated aggregation during the maximum phase probably cleared even lithogenic particles and, second, the reduction in grazing pressure allowed phytoplankton aggregates to sink freely, without processing by zooplankton, thus enhancing organic carbon exportation.

3.5.3. Vertical particle transfer towards mesopelagic depths

As highlighted in Section 3.5.1 there is a substantial difference between the amount of particles arriving at 900 m and 400 m traps in ALB-2, as illustrated by TWF (Table 3.3). Most of the dissimilitude is due to the lower amount of particles reaching the 900 m trap at intervals of high particulate fluxes in the 400 m trap (Fig. 3.6). The opposite situation, however, has been observed by the end of April, when ALB-2-I (900 m) fluxes were slightly higher than those recorded at the shallower ALB-2-S trap. This anomalous situation could relate to the low particle settling speed during that epoch, which delayed the arrival of particles to 900 m depth, in parallel with a trend towards minimum fluxes in surface waters.

About the high flux period in May, various processes in the water column could account for the observed dramatic particle flux decrease with depth.

Particle aggregates are subject to degradation by physical disaggregation and chemical dissolution, but these processes would play a minor role on fast sinking aggregates. Biological processes

could play a major role and seem to cause rapid turnover of aggregated material. Biological processes are dominated by bacterial colonisation leading to remineralization and solubilization, and by protozoans that feed on both bacteria and other aggregate components. Mesozooplankton and fish feed, respectively, on aggregate constituents and on intact aggregates, thus causing their disintegration or complete sequestration and remineralization (Kiørboe, 2001). Settling of organic-rich particulate matter through LIW jointly with the high oxygen utilisation rates linked with microbial degradation have been claimed responsible for the formation of the most intense oxygen minimum zone of the Mediterranean in the centre of the WAG (Packard et al., 1988).

The coherence in the biogenic elemental ratios of ALB-2-S and ALB-2-I traps demonstrates that degradation processes have a higher impact on the amount of settling material than on its composition. This is because, due to the short transfer times, degradation affects only the weakest constituents in the aggregates, i.e. binding material such as mucus feeding webs, appendicularian houses and so on. Since this binding material plays a determinant role in particle aggregation, weaker aggregates may selectively disintegrate. The resulting aggregate fragments and individual particles may reduce their settling speed drastically -even down to zero- and, therefore, could remain suspended in the water column for long time thus precluding their transfer to deeper areas. The LIW and WMDW sluggish steady westward flow in the WAB probably provides a permanent mechanism for exporting suspended particles and dissolved substances resulting from the degradation of sinking particles.

Offshore advection of phytoplankton-rich water masses, enhanced particulate fluxes driven by aggregation in the centre of the WAG, mesopelagic degradation with depth, and westward exportation of particulate and dissolved organic matter through the Strait of Gibraltar make the WAB an efficient system of organic matter transfer from coastal zones in the Alboran Sea towards deep areas in the near Atlantic Ocean. Biogenic and lithogenic suspended particulate matter originated in surface waters in the Mediterranean has been recently identified in the deep outflow of Mediterranean water west of Gibraltar Strait by Freitas and Abrantes (2002).

3.5.4. Near bottom particle transfer

Notwithstanding the general reduction in particle fluxes with depth during the studied period, near bottom traps recorded higher time weighed and instantaneous fluxes than any of the traps located at intermediate depths. On average, TWF values near the bottom doubled, the values recorded at intermediate depths. This is a long-term trend as identified in the year round monitoring experiment embedding the HFF experiment described in the present paper. Fabres et al. (2002) concluded that the near bottom flux increase was caused by downslope transport related to eddy-like activity close to the seafloor. The analysis of high-resolution data presented here brings further light to that relationship.

The time flux evolution highlights the relevance of downslope transport as the maximum opal and organic matter fluxes are within the range of the highest fluxes recorded in the traps at 400-500 m, but well above the values of the fluxes recorded at the 900 m depth ALB-2-I trap. Lithogenic and

carbonate fluxes are distinctly higher near bottom, thus evidencing the supply of benthic layer resuspended particles from upslope areas. Local sediments are mostly made of lithogenic (70-80 %) and carbonate (20-30%) particles, with a minor organic matter fraction (Masque et al., in press). This is in accordance with the relative abundances of the main constituents, as organic matter and opal are lower and the lithogenic fraction is higher at near bottom traps than in intermediate traps.

Despite their striking differences, intermediate depth and near bottom fluxes are still somehow coupled. This coupling is marked by the similar evolution of TMF, organic matter, opal and lithogenic fraction fluxes and relative abundances, and Si/N and Si/C ratios (Figs. 3.5, 3.6 and 3.9). Elemental ratios provide valuable information on the transfer of particulate matter reaching the WAB seafloor. Si/N (1.5-2.5) and Si/C (0.15-0.25) fluctuate around background values during April, show noticeable increases (2.5-3 for Si/N and 0.30-0.35 for Si/C) at the beginning of May that parallel those recorded in surface traps, and remain high for the rest of the experiment (Fig. 3.12).

It is worth reminding that maximum fluxes at surface traps held the highest Si/N and Si/C ratios. The observed evolution of near bottom biogenic ratios is likely caused by the episodic fast settling of material from the sea surface towards the shelf and upper slope seafloor surrounding the study site, where it may accumulate temporarily as a fluffy non-cohesive layer on the seabed. During and after its arrival to the bottom, this fresh, highly biogenic material is transferred close to the seafloor, jointly with previously accumulated particles, towards lower slope areas. The hydrographic sections shown on Figure 3.3 reveal lower light transmission just over the bottom along the continental slope, thus supporting the near bottom transfer of particulate material. The mixing of the particulate matter coming from the overlying waters with the material already accumulated on the bottom accounts for the higher compositional homogeneity of near bottom particle fluxes (Heussner et al., 1999). The accumulation of surface-derived material on the seafloor of shallower areas and its sustained downslope transfer explains the broad nature of the flux peaks and the persistence of high biogenic ratios long after surface trap ratios have dropped again to background values. This interpretation is substantiated by the work from other authors (i.e. Lampitt, 1985; Walsh et al., 1988) who considered the contribution to near bottom fluxes of resuspended particles accumulated in a fluff layer resulting from enhanced export events from surface waters.

Higher opal and organic matter fluxes in ALB-E-F and ALB-D-F than in ALB-1-F could be caused by the position of the later station on the flank of a smooth bulge where, possibly, less resuspended material from upslope shallower areas arrives. The marked flux decrease with water depth implies that shallower areas should receive and store higher amounts of biogenic-rich particulate matter for potential downslope transfer. Varied source areas may explain punctual compositional differences in the transferred material. The higher average Si/N and Si/C ratios in ALB-E-F with respect to the rest of the near bottom traps may be due to the accumulation of organic material that underwent more intense grazing in the upper water column (Dugdale et al., 1995). The location of ALB-E-F could favor the arrival of particles via the passage connecting the marginal depression north of the Djibouti Bank and the WAB (see Fig. 3.1b). The highly productive conditions on the surface waters north of Djibouti Bank during a longer period (see SeaWiFS from 23/04 to 27/04, Figs. 3.2c and 3.2d) could lead to the development of a larger zooplankton population that fed on the phytoplankton stock thus leaving less

ungrazed cells to sink out of the surface layer. The relation between the establishment of high productivity conditions and the delayed development (days or weeks) of a zooplankton grazing community has been identified in the nearby Almeria-Oran Front by Thibault et al. (1994).

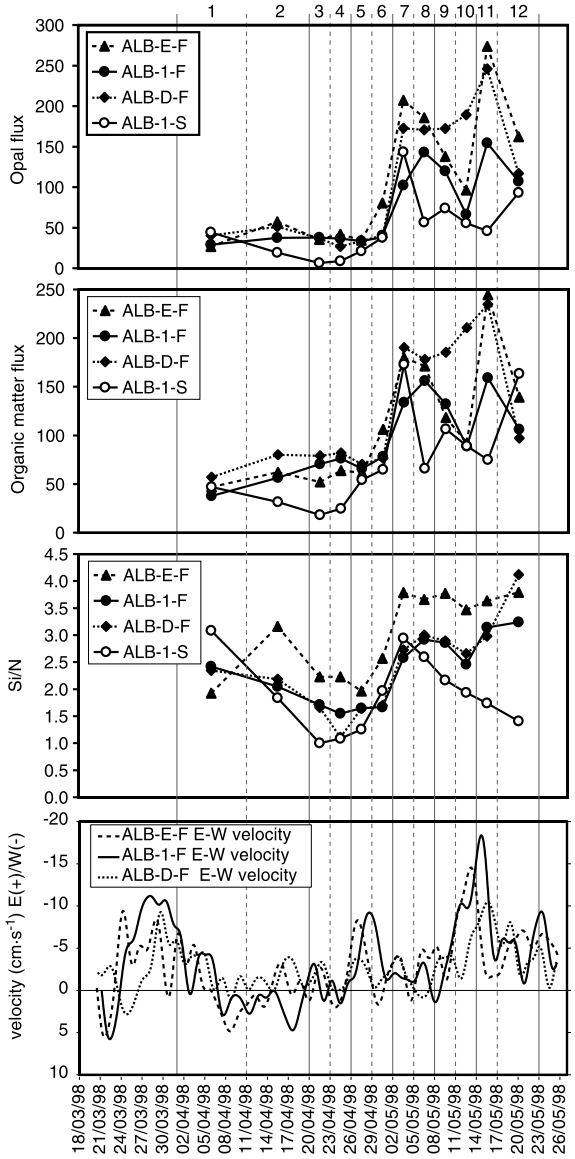

Figure 3.12. Comparison of the temporal evolution of opal fluxes, organic matter fluxes, and Si/N ratios from near bottom traps ALB-E-F, ALB-1-F and ALB-D-F with the E-W low pass-filtered component of the current at the same stations. Fluxes are expressed in mg·m^{-2}·day^{-1} and current speed in cm·s^{-1}.

Furthermore, the comparison of near bottom fluxes and their composition brings further light on the mechanisms and factors controlling the transfer and redistribution of newly arrived material. Figure 3.12 presents the filtered E-W current component recorded at the three near bottom stations located from 954 to 976 meters depth (Table 3.1) and compares it with the opal flux, the organic matter flux and the Si/N ratio of the same stations plus ALB-1-S as a reference. Almost synchronously to the first major flux pulse recorded in ALB-1-S, between 02/05 and 05/05, the three near bottom traps also recorded a noticeable pulse of highly biogenic particles. This simultaneous arrival of material to both depths proves that the sequence of vertical export from surface waters, bottom deposition and downslope transfer by

resuspension is rapid. The fact that ALB-E-F started recording the pulse even slightly earlier than ALB-1-S reinforces the above hypothesis about a different source area for ALB-E-F. Organic-rich particles were probably arriving at ALB-E-F source area earlier than they did to the source areas of the other two traps. Near bottom fluxes remained high for at least 3 days after diminution of the pulse in surface waters. From 08/05 onwards fluxes were noticeably reduced in ALB-1-F and ALB-E-F. This reduction matches an increase of the westward current speed at the same stations, where values higher than 10 $cm \cdot s^{-1}$ were reached. It is remarkable that neither the flux reduction nor the above 10 $cm \cdot s^{-1}$ pulse of the westward current were recorded on ALB-D-F, which fluxes remained high. Just after the deceleration of the westward current, between 14/05 and 17/05, fluxes increased to absolute maxima in all bottom traps to dramatically drop in the last sample. Even if some hydrodynamic biases can not be completely ruled out, and even though we cannot draw a cause-effect relationship due to the shortness of the record, it is likely that pulses in current speed above a given threshold enhance transportation versus settling thus causing fluxes to decrease. Moreover, the consecutive lowering in current speed would favour the high amount of resuspended particles to settle down thus determining fluxes to peak. Biscaye and Anderson (1994) suggested a relation between near bottom fluxes and turbulent energy to explain flux variability at different slope locations in the Mid Atlantic Bight. In our HFF experiment, the last flux decrease seems to exclude such an interpretation although it must be considered that the exhaustion of fluffy material available for resuspension in shallower areas may also cause a decrease in near bottom fluxes.

Fluxes and specially Si/N and Si/C ratios recorded in the remaining near bottom trap (ALB-2-F, Fig.3.10) are delayed 3 days with respect to the other near bottom traps. This indicates the time resuspended particles need to travel from midslope (~1000 m) to the lower continental slope (~1300 m).

On top of the mesopelagic depth withdrawal described in Section 3.5.3, the enhanced deep transfer and the near bottom redistribution of biogenic-rich material constitute a mechanism to effectively remove substantial amounts of organic carbon from surface waters and to transfer it towards the deep sediment permanent reservoir. This mechanism has profound implications for paleoceanographic and paleoclimatologic studies based on sediment records collected at the deepest part of restricted basins as the WAB. Our work shows that such sediment records may register reliably the productive events that occurred in surface waters basin-wide.

3.6. Summary and conclusions

The HFF experiment in the WAB shows the potential of multidisciplinary high-resolution studies to contribute to the understanding of the mechanisms of particle flux biophysical coupling and the efficiency of the biological pump in marginal seas. From the previous discussion a series of conclusions can be extracted and summarised as follows.

Particle settling speeds during the studied period ranged from ~80 $m \cdot d^{-1}$ to more than 300 $m \cdot d^{-1}$.

Enhanced biogenic-rich particulate fluxes to intermediate depths in the northern sector of the WAG resulted from the combination of three main processes:

1. Upwelling-related augmentation of the primary production and development of a significant diatom community in surface waters outside the WAG.

2. Development of small instabilities, in the form of eddies, on the edge of the WAG causing a centripetal advection of phytoplankton (diatom)- rich water masses along isopycnal surfaces.

3. Major physical and biologically-mediated aggregation processes acting on the advected phytoplankton stock. Microphagous zooplankton grazing would have played a major role in repackaging and reprocessing such phytoplankton stocks.

These aggregation processes efficiently scavenged lithogenic particles from the water column leading to a reduction in their abundance at the end of the particle bloom events.

A noticeable withdrawal of particles travelling between 400 and 900 meters in the centre of the WAG has been noted concurrently with particle flux enhancement at intermediate depths. This flux reduction was probably linked to disaggregation and particle size reduction due to bacterial and biological activity and to the physical advection by a deep waters westward sluggish flow. Besides this noteworthy sequestration of organic-rich material through the water column, a relevant near bottom transfer of material accumulated in shallower areas has been noticed.

Both processes constitute a mechanism by which carbon can be effectively removed from surface waters and, driven to deep-water levels or accumulated in deep-sea sediments. The latter process suggests that the sedimentary record in the deep Alboran Sea may accurately record past productivity events that occurred in surface waters basin-wide.

Acknowledgements

Authors would like to thank the Elemental Analysis, the ICP-AES and the Chemistry Laboratory teams of the “Serveis Científico Tècnics” of University of Barcelona that provided invaluable help in carbon-nitrogen and silica analyses. We thank Francisco Plaza from University of Malaga for processing the CTD data. We are grateful to Frederic Melin from the Marine Environment Unit (ME) of the Space Applications Institute (SAI) for providing us with the SeaWiFS images and to Pedro Arnau for letting us use his software to browse the SST images. José Luis Casamor also helped us by providing the 3D image on Figure 3.1. We are finally indebted with the officers, crew, technicians and scientists on board R/V Garcia del Cid and R/V Hespérides during the various MATER cruises for their help and dedication. J. F. was supported by an FPU grant (AP95 44002743) from “Ministerio de Educación y Ciencia”. The body of the research was supported by the EU MTPII-MATER project (MAS3-CT96-0051) to which the Spanish “Comisión Asesora de Investigación Científica y Técnica” and the Catalan “Comissió Interdepartamental per la Recerca i la Investigació Tecnològica” provided substantial co-funding and the

EU ADIOS project (EVK3-CT-2000-00035). GRC Geociències Marines is additionally funded by "Generalitat de Catalunya" through its excellency research groups program (ref. 1999 SGR-63) and the Thematic Network "Barcelona Consortium on Marine Geosciences" (1999 XT-0025). Spanish postgraduates fight for better employment rights, http://www.precarios.org.

References

Alldredge, A.L., Silver, M.W., 1988. Characteristics, dynamics and significance of marine snow. Progress in Oceanography 20, 41-82.

Alldredge, A.L., Gotschalk, C.C., 1989. Direct observations of the mass flocculation of diatom blooms: Characteristics, settling velocities and formation of diatom aggregates. Deep-Sea Research 36, 159-171.

Allen J.T., Smeed D.A, Tintore J., Ruiz S., 2001. Mesoscale subduction at the Almeria-Oran front. Part 1: Ageostrophic flow. Journal of Marine Systems 30, 263-285.

Arin L., Morán X.A.G., Estrada, M., 2002. Phytoplankton size distribution and growth rates in the Alboran Sea (SW Mediterranean): Short-term variability related to mesoscale hydrodynamics. Journal of Plankton Research,24, 1019-1033.

Baker, E.T., Milburn, H.B. Tennant, D.A., 1988. Field assessment of sediment trap efficiency under varying flow conditions. Journal of Marine Research 46, 573-592.

Baldacci, A., Corsini, G., Grasso, R., Manzella, G., Allen, J. T., Cipollini, P., Guymer, T.H., Snaith, H. M., 2001. A study of the Alboran sea mesoscale system by means of empirical orthogonal function decomposition of satellite data. Journal of Marine Systems 29, 293-311.

Berelson, W.M., 2002. Particle settling rates increase with depth in the ocean. Deep-Sea Research II 49, 237-251.

Biscaye, P.E., Anderson, R.F., 1994. Fluxes of particulate matter on the slope of the southern Middle Atlantic Bight: SEEP-II. Deep-Sea Research II 41, 459-509.

Bory, A., Jeandel, C., Leblond, N., Vangriesheim, A., Khripounoff, A., Beaufort, L., Rabouille, C., Nicolas, E., Tachikawa, K., Etcheber, H., Buat Menard, P., 2001. Downward particle fluxes within different productivity regimes off the Mauritanian upwelling zone (EUMELI program). Deep-Sea Research I 48, 2251-2282.

Brzezinski, M.A., 1985. The Si:C:N ratio of marine diatoms: interspecific variability and the effect of some environmental variables. Journal of Phycology 21, 347–357.

British Oceanographic Data Centre, 1994. General bathymetric chart of the oceans (GEBCO): Birkenhead, Merseyside, England, Bidstone Obs (CD-ROM).

Cushman-Roisin, B., 1994. Introduction to geophysical fluid dynamics. Prentice-Hall, Englewood Cliffs UK, 320 pp.

Ducklow, H.W. Steinberg ,D.K., Buesseler K.O., 2001. Upper ocean carbon export and the biological pump. Oceanography, 14, 50-58

Dugdale, R.C, Wilkerson, F.P, Minas, H.J., 1995. The role of silicate pump in driving new production. Deep-Sea Research I 42, 697-719.

Earth Resources Information Systems Data Center, 1996. Global 30 seconds arc elevation dataset: Sioux Falls, South Dakota, U.S. Geological Survey (http://edcwww.cr.usgs.gov/lansdaac/gtopo30/gtopo30.html).

Fabres, J., Calafat, A., Sanchez-Vidal, A., Canals, M., Heussner, S., 2002. Composition and spatio-temporal variability of particle fluxes in the Western Alboran Gyre, Mediterranean Sea. Journal of Marine Systems 33-34, 431-456.

Fielding S., Crisp N., Allen J.T., Hartman M.C., Rabe B., Roe H.S.J., 2001. Mesoscale subduction at the Almeria-Oran front. Part 2: Biophysical interactions. Journal of Marine Systems 30, 287-304.

Fortier, L., Le Fevre, J., Legendre, L., 1994. Export of biogenic carbon to fish and to the deep ocean: The role of large plankton microphages. Journal of Plankton Research 16, 809-839.

Freitas P.S., Abrantes, F., 2002. Suspended particulate matter in the Mediterranean water at the Gulf of Cadiz and off the southwest coast of the Iberian Peninsula. Deep-Sea Reasearch II 49, 4245-4261.

Garcia-Gorriz, E., Carr, M.E., 1999. The climatological annual cycle of satellite-derived phytoplankton pigments in the Alboran Sea. Geophysical Research Letters 26, 2985-2988.

Garcia-Gorriz, E., Carr, M.E., 2001. Physical control of phytoplankton distributions in the Alboran Sea: A numerical and satellite approach. Journal of Geophysical Research, C 106, 16795-16805.

Garcia Lafuente, J.G., Cano, N., Vargas, M., Rubin, J.P., Hernandez Guerra, A., 1998. Evolution of the Alboran Sea hydrographic structures during July 1993. Deep-Sea Research I 45, 39-65.

Gardner, W. D., Biscaye, P. E., Richardson, M.J., 1997. A sediment trap experiment in the Vema Channel to evaluate the effect of horizontal particle fluxes on measured vertical fluxes. Journal of Marine Research 55, 995-1028.

Gomis, D., Ruiz, S., Pedder, M. A., 2001. Diagnostic analysis of the 3D ageostrophic circulation from a multivariate spatial interpolation of CTD and ADCP data. Deep-Sea Research I 48, 269-295.

Gorsky, G., Prieur, L., Taupier-Letage, I., Stemmann, L., Picheral, M., 2002. Large particulate matter in the Western Mediterranean I. LPM distribution related to mesoscale hydrodynamics. Journal of Marine Systems 33-34, 289-311.

Hansen, J.L.S., Kiørboe T., Alldredge, A.L., 1996. Marine snow derived from abandoned larvacean houses: sinking rates, particle content and mechanisms of aggregate formation. Marine Ecology Progress Series 141, 205-215.

Heburn, G.W., La Violette, P.E., 1990. Variations in the structure of the anticyclonic gyres found in the Alboran Sea. Journal of Geophysical Research C 95, 1599-1613.

Heussner, S., Ratti, C., Carbonne, J., 1990. The PPS 3 time-series sediment trap and the trap sample techniques used during the ECOMARGE experiment. Continental Shelf Research 10, 943-958.

Heussner, S., Durrieu de Madron, X., Radakovitch, O., Beaufort, L., Biscaye, P.E., Carbonne, J., Delsaut, N., Etcheber, H., Monaco, A., 1999. Spatial and temporal patterns of downward particle fluxes on the continental slope of the Bay of Biscay (Northeastern Atlantic). Deep-Sea Research II 46, 2101-2146.

Kiørboe, T., 2001. Formation and fate of marine snow: small-scale processes with large-scale implications. In: J.M. Gili, J.L. Petrus and T.T. Packard (eds.) A marine science odyssey into the 21st century. Scientia Marina 65 (Suppl.2), 57-71

La Violette, P.E., 1984. The advection of submesoscale thermal features in the Alboran Sea Gyre. Journal of Geophysical Research 14, 550-565.

La Violette, P.E., 1986. Short-term measurements of surface currents associated with the Alboran Sea Gure during Donde Va?. Journal of Physical Oceanography 16, 262-279.

La Violette, P.E., 1995. Overview of the major forcings and water masses of the Western Mediterranean Sea. In: P. E. La Violette (Editor), Seasonal and interannual variability of the western Mediterranean Sea (Coastal and Estuarine Studies, 46). American Geophysical Union, Washington DC, USA, pp. 1-11.

La Violette, P.E., Arnone, R., 1998. Variations in time and space scales in the physical and bilogical characacter of the Mediterranean Sea. Rapports et procés verbaux des réunions; Commission internationale pour l'exploration scientifique de la Mer Méditerranée 35, 114-119

Masque, P. Fabres, J., Canals, M., Sanchez-Cabeza, J.A., Sànchez-Vidal, A., Cacho, I., Calafat, A.M. Bruach, J.M. Accumulation rates of major constituents of hemipelagic sediments in the deep Alboran Sea: a centennial perspective of sedimentary dynamics. Marine Geology, In press.

McClain, E.P., Pichel W.G., Walton, C.C., 1985. Comparative performance of AVHRR- based multichannel sea surface temperatures. Journal of Geophysical Research, C 6, 11587-11601.

Melin, F., 2000. SeaWiFS images archive, SeaWiFS dataset for the Eastern Atlantic. September 1997-May 1998. Space Applications Institute (SAI), Marine Environment Unit (ME), Joint Research Centre (JRC), online dataset http://me-www.jrc.it/me-website/contents/shared_utilities/frames/archive_seawifs.htm.

Melin, F., Bulgarelli, B., Gobron, N., Pinty, B., Tacchi, R., 2000. An integrated tool for SeaWiFS operational processing. Joint Research Centre Publication, No. EUR 19576 EN. Space Applications Institute (SAI), Marine Environment Unit (ME), Joint Research Centre (JRC).

Minas, H.J., Coste, B., Le Corre, P., Minas, M. Raimbault, P., 1991. Biological and geochemical signatures associated with the water circulation through the Strait of Gibraltar and in the Western Alboran Sea. Journal of Geophysical Research C 96, 8755-8771.

Moran, X.A.G., Estrada, M., 2001. Short-term variability of photosynthetic parameters and particulate and dissolved primary production in the Alboran Sea (SW Mediterranean). Marine Ecology Progress Series 212, 53-67.

Packard, T.T., Minas, H.J., Coste, B., Martinez, R., Bonn, M.C., Gostan, J., Garfield, P., Christensen, J., Dortch, Q., Minas, M., Copin-Montegut, G., Copin-Montegut, C., 1988. Formation of the Alboran oxygen minimum zone. Deep-Sea Research 35, 1111-1118.

Parrilla, G., Kinder, T.H. Preller, R.H., 1986. Deep and Intermediate Mediterranean Water in the western Alboran Sea. Deep-Sea Research 33, 55-88.

Peinert, R., Miquel, J.C., 1994. The significance of frontal processes for vertical particle fluxes: A case study in the Alboran Sea (SW Mediterranean Sea). Journal of Marine Systems 5, 377-389.

Perkins, H., Kinder, T., La Violette, P.E., 1990. The Atlantic inflow in the western Alboran Sea. Journal of Physical Oceanography 20, 242-263.

Pistek, P., De Strobel, F., Montanari, C., 1985. Deep-sea circulation in the Alboran Sea. Journal of Geophysical Research C 90, 4969-4976.

Plaza, F., 2001. Variabilidad temporal en la Cuenca Occidental del Mar de Alborán y su relación con los flujos a través del Estrecho de Gibraltar y Pasaje de Alborán. Ph.D. Thesis. Univ. Cádiz, Spain, unpublished.

Rodriguez, J., Blanco, J.M., Jimenez Gomez, F., Echevarria, F., Gil, J., Rodriguez, V., Ruiz, J., Bautista, B., Guerrero, F., 1998. Patterns in the size structure of the phytoplankton community in the deep fluorescence maximum of the Alboran Sea (southwestern Mediterranean). Deep-Sea Research I 45, 1577-1593.

Ruiz, J., Echevarria, F., Font, J., Ruiz, S., Garcia, E., Blanco, J.M., Jimenez Gomez, F., Prieto, L., Gonzalez Alaminos, A., Garcia, C.M., Cipollini, P., Snaith, H., Bartual, A., Reul, A., Rodriguez, V., 2001. Surface distribution of chlorophyll, particles and gelbstoff in the Atlantic jet of the Alboran Sea: from submesoscale to subinertial scales of variability. Journal of Marine Systems 29, 277-292.

Sarhan, T., García Lafuente, J., Vargas, M., Vargas, J. M. Plaza, F., 2000. Upwelling mechanisms in the Northwestern Alboran Sea. Journal of Marine Systems 23, 317-331.

Sparnocchia, S., Manzella, G.M.R., La Violette P.E., 1995. The interannual and seasonal variability of the MAW and LIW core properties in the Western Mediterranean Sea. In: P. E. La Violette (Editor), Seasonal and interannual variability of the western Mediterranean Sea (Coastal and Estuarine Studies, 46). American Geophysical Union, Washington DC, USA, pp. 177-194.

Takahashi, K., 1986. Seasonal fluxes of pelagic diatoms in the subartic Pacific, 1982-1983. Deep-Sea Research 33, 1225-1251.

Thibault, D., Gaudy, R., Le Fèvre, J., 1994. Zooplankton biomass, feeding and metabolism in a geostrophic frontal area (Almeria-Oran Front, western Mediterranean). Siginificance to pelagic food webs. Journal of Marine Systems 5, 297-311.

Viudez, A., Tintore, J., Haney, R.L.1996. Circulation in the Alboran Sea as determined by quasi-synoptic hydrographic observations. Part I: Three-dimensional structure of the two anticyclonic gyres. Journal of Physical Oceanography, 26, 684-705.

Viudez, A., Pinot, J.-M., Haney, R.L., 1998. On the upper layer circulation in the Alboran Sea. Journal of Geophysical Research C 103, 21653-21666.

Vives, F., Santamaria, G., Trepat, I., 1975. El zooplancton en los alrededores del estrecho de Gibraltar en junio.julio de 1972. Resultados expediciones científicas del buque oceanográfico Cornide de Saavedra 4, 7-100.